國立交通大學

資訊工程系

碩 士 論 文

應用於無線基頻處理器之可適應等化器設計

Design of Pilot-based Adaptive Equalization
for Wireless OFDM Baseband Applications

研 究 生：吳明曄

指導教授：許騰尹　教授

中 華 民 國 九 十 四 年 九 月

應用於無線基頻處理器之可適應等化器設計
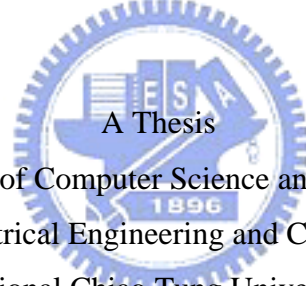# Design of Pilot-based Adaptive Equalization for Wireless OFDM Baseband Applications

研 究 生：吳明曄　　　　Student：Ming-Yeh Wu

指導教授：許騰尹　　　　Advisor：Terng-Yin Hsu

國 立 交 通 大 學
資 訊 工 程 系
碩 士 論 文

A Thesis
Submitted to Department of Computer Science and Information Engineering
College of Electrical Engineering and Computer Science
National Chiao Tung University
in partial Fulfillment of the Requirements
for the Degree of
Master
in

Computer Science and Information Engineering

September 2005

Hsinchu, Taiwan, Republic of China

中華民國九十四年九月

應用於無線基頻處理器
之可適應等化器設計

學生：吳明曄　　　　　　　　指導教授：許騰尹 博士

國立交通大學資訊工程學系碩士班

摘要

　　本論文研製之可適應等化器不但增強對抗一般多重路徑通道效應，更大大增強了對奇異性的多重路徑通道效應之抵抗力，而所提出之相位雜訊偵測與補償機制則大幅增加了對相位雜訊影響之容忍度。一般傳統的等化器一遇到所謂的奇異性多重路徑最大的問題就是在補償訊號的同時會增強雜訊，因此整個系統的效能往往被拖垮，因此我們提出了一個以導引信號為判斷依據然後於每段正交分頻多工符元更新一次的可適應等化器，在 2.4 GHz 的頻帶、IEEE 衰減通道均方根延遲範圍 50 ns 的條件下，整體系統的效能比參考的演算法有高達 6 dB 左右的提升。

　　而考慮相位雜訊時這整個問題又不是如此單純了，系統效能隨著相位雜訊變大而嚴重衰減，因此我們發展出另一個結合相位雜訊與載波相位偏移的訊號模型，同時提出了一個相位雜訊偵測與結合載波相位偏移的補償架構。此演算法擴展了對相位雜訊的抵抗能力：從最大迴路頻寬 7 ppm、最大迴路時間常數 1.1 kHz 至 11 ppm、25 kHz。

Design of Pilot-based Adaptive Equalization for Wireless OFDM Baseband Applications

Student: Ming-Yeh Wu   Advisor: Dr. Terng-Yin Hsu

Department of Computer Science and Information Engineering, National Chiao Tung University

Abstract

A procedure against heavy multipath is developed in this thesis, which also can handle the ordinary multipath. Besides, another mechanism is proposed to extending the phase noise tolerance. The biggest problem of the conventional 1-tap equalizer is that it will enhance the noise while correcting the received signal once the singular channel occurs. Hence, we propose a pilot-based adaptive channel equalization that will update the channel information every OFDM symbol. In 2.4 GHz, the overall system performance gain is about 6 dB compared with the reference design for IEEE channel model with RMS delay spread 50 ns and 13 taps.

Considering the phase noise, it is not so easy. Obviously, the system performance dramatically degrades when the phase noise increases. Therefore, we develop a new CFO joint phase noise model. The phase noise detection and compensation architectures are proposed at the same time. This algorithm extends the tolerance of phase noise from maximum loop bandwidth 7 ppm, maximum loop time constant 1.1 kHz to 11 ppm and 25 kHz in respectively.

Acknowledgement

Contents

List of Figures *page*

List of Tables $\qquad$ *page*

CHAPTER 1

INTRODUCTION

Orthogonal Frequency Division Multiplexing (OFDM) is a kind of spectrally efficient signaling technique for communications over frequency selective fading channels [11], which has been adopted by many transmission systems, e.g., WLAN systems based on IEEE802.11a/g [1], [3], digital audio broadcasting (DAB) [21], and digital video broadcasting terrestrial TV (DVB-T) [22]. Unfortunately, OFDM systems are sensitive to imperfect synchronization and non-ideal front-end effect, caused serious system performance degradation. It also causes strict front-end specifications and results in expensive front-end circuits. Generally, OFDM is highly sensitive to carrier frequency offset (CFO) between transmitter and receiver, which is caused by a Doppler shift of the radio frequency (RF) carrier, the mismatch of local oscillator (LO) between the transmitter and the receiver or phase noise of an oscillator. Frequency offset can introduce inter-carrier interference (ICI) in an OFDM receiver due to the loss of the orthogonality between sub-carriers and severely degrade the overall system performance if without appropriate correction. In order to prevent performance degradation, OFDM systems pay a cost of strict front-end specifications and expensive front-end implementations.

Recently, some researches have focused on the development of equalizer, especially for low cost technology. Among of different receiver architectures, direct divider architecture is one popular candidate for simply implementation. However, this easy mechanism is also suffered from their own impairments, such as singular

channel problem, which is due to the unstable poles of the channel frequency response (CFR). More specifically, it occurs when noise is enlarged that received signal is not exactly compensated and causes error.

In order handle the multipath, a number of adaptive methods for OFDM systems have been proposed. Although these time domain methods can work well under severe multipath, they don't take the singular channel into considerations, and then the estimation error will be enlarged when the disturbing situation is introduced into the system. In [12], the proposed algorithm has considered narrowband interference, but the channel condition is ambiguous and the simulation result is insufficient. A blind algorithm [14] is developed, however it doesn't guarantee the convergence condition of the estimation when the packet based WLAN standards are considered. In [13], a pilot-based algorithm is introduced, whose accuracy maybe acceptable, but the computing cost is too high to be suitable for hardware implementation. A GI-based LMS algorithm is proposed in [15], where it pays low cost of computational complexity for operations. However, the channel condition is too easy and the performance is the worst among these methods.

Practically, CFO and phase noise will jointly occur and greatly degrade the system performance. The effects of phase noise not only introduce the unwanted random phase into the desired signal but also limit the accuracy of the CFO estimation. There are also many methods proposed to compensate the phase noise so far. An phase noise correction scheme is proposed in [23], but it does not totally solve this problem.

First, an adaptive equalization is proposed for special channel condition. This method uses the pilots as criterion. Then considering the joint impairments of CFO and phase, a phase noise estimation algorithm which is suitable for implementation issue is developed to overcome the large performance degradation caused by phase

noise. In the proposed algorithm, it utilizes pilots in frequency domain, which are rotated by additional frequency offset and phase noise, to carry out the phase noise parameter estimation. The scheme can tolerate loop bandwidth up to 11 ppm and loop time constant 25 kHz. From simulation results, it is clear to see that the performance of the proposed scheme is better than the reference designs, thus it can achieve a high performance receiver.

In this thesis, carrier frequency offset, sampling clock offset and phase noise are three synchronization issues. And multipath is also need to be taken into account. The effects of them will be introduced in the next chapter. The estimation and compensation methods will be introduced in chapter 3. We simulate and realize the proposed method on a WLAN system, i.e. IEEE 802.11g. In chapter 2, we will introduce the IEEE 802.11g standard and the MATLAB simulation platform. The simulation results and comparison will be presented in chapter 4. The proposed method can be used in a real WLAN system. In chapter 5, we will introduce the design flow from high level description to low level architecture and hardware. The fixed point simulation results and hardware architecture will be introduced in that chapter. Finally, chapter 6 is the conclusion and future work.

Chapter 2
SYSTEM PLATFORM

In this chapter, we are going to describe three blocks of wireless communications, transmitter, channel model, and receiver. At first, we introduce the basic of OFDM and the IEEE 802.11g PHY specification, which combines both 802.11a (OFDM) and 802.11b (DSSS) at one system. And then we present the IEEE 802.11g PHY transmitter block diagram. After that, we characterize some wireless channel models and parameters, such as additive white Gaussian noise (AWGN), carrier frequency offset (CFO), multi-path, and so on. Finally, we propose a universal receiver system model.

2.1 IEEE 802.11g PHY Specification

Orthogonal Frequency Division Multiplexing (OFDM) is a multi-carrier modulation that achieves high data rate and combat multi-path fading in wireless networks. The main concept of OFDM is to divide available channel into several orthogonal sub-channels. All of the sub-channels are transmitted simultaneously, thus achieve a high spectral efficiency. Furthermore, individual data is carried on each sub-carrier, and this is the reason the equalizer can be implemented with low complexity in frequency domain.

The 802.11g PHY defined in standard is known as the Extended Rate PHY (ERP), operating in the 2.4 GHz ISM band. Four operational modes are listed as followed:

A. ERP-DSSS/CCK – This mode builds on the payload data (PSDU) rates of 1, 2, 5.5, and 11 Mbit/s that use DSSS (DBPSK and DQPSK), CCK and optional PBCC modulation, and the PLCP Header operates on data rate 1 Mbit/s DBPSK for Long SYNC, 2 Mbit/s DQPSK for Short SYNC. Figure 2.1 shows the format for the interoperable PPDU that is the same with 802.11b PPDU format, and the details of components such as spreading code, scrambler, CRC implementation, and modulation refer to 802.11b standard.
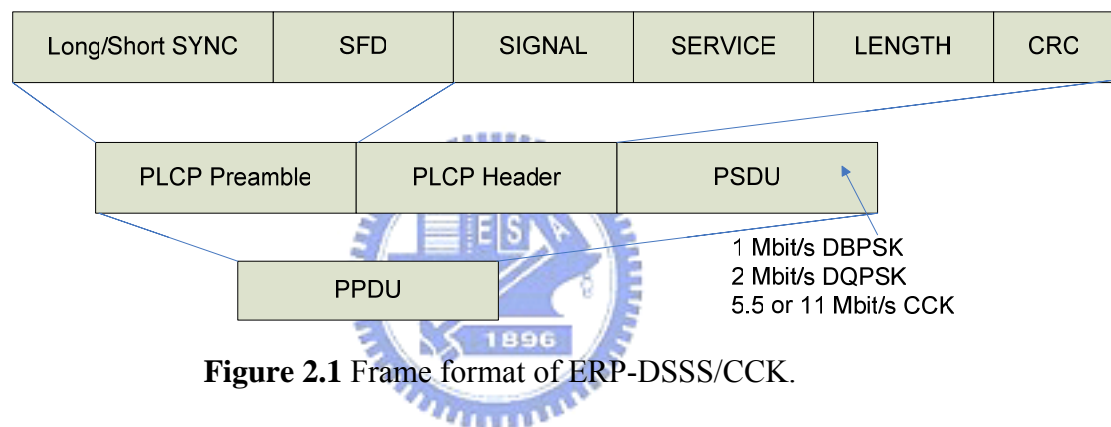
Figure 2.1 Frame format of ERP-DSSS/CCK.

B. ERP-OFDM – This mode builds on the payload data rates of 6, 9, 12, 18 24, 36, 48, and 54 Mbit/s, based on different modulations (PSK and QAM) and coding rate, by means of OFDM technique. Except PLCP Preamble, SIGNAL field with data rate 6 Mbit/s and DATA are packaged (OFDM) symbol by symbol. The only difference from 802.11a is the operating ISM band (802.11a is in 5 GHz). Figure 2.2 is the PPDU format.
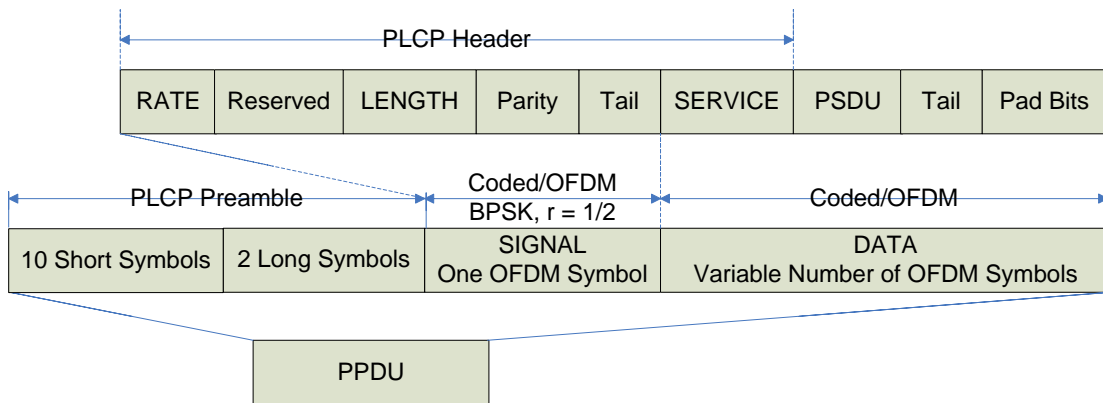
Figure 2.2 Frame format of ERP-OFDM.

C. ERP-PBCC – This mode builds on the payload data (PSDU) rates of 22 and 33 Mbit/s and it is a single-carrier modulation scheme that encodes the payload using 256-state packet binary convolutional code. The PPDU format follows mode A).

D. DSSS-OFDM – This mode is a hybrid modulation combining a DSSS preamble and header with an OFDM long preamble, signal field and payload transmission. In the boundary between DSSS and OFDM parts, it is single carrier to multi-carrier transition definition. The payload data rates are the same with those of B). The PPDU format is as followed in Figure 2.3.
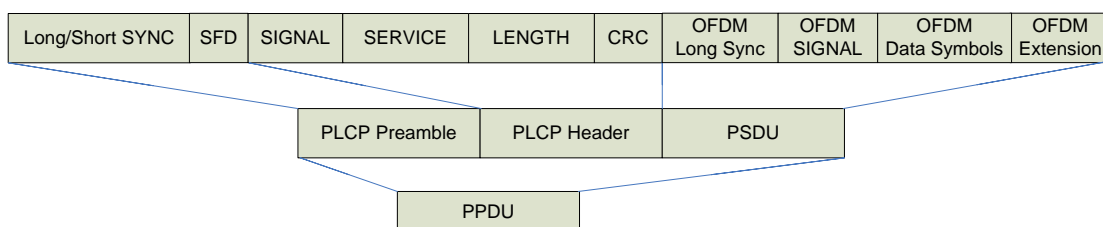
Figure 2.3 Frame format of DSSS-OFDM.

An ERP BSS is capable of operating in any combination of available ERP modes

and Non ERP modes. For example, if options are enabled, a BSS could operate in an ERP-OFDM-only mode, a mixed mode of ERP-OFDM and ERP-DSSS/CCK, or a mixed mode of ERP-DSSS/CCK and Non-ERP. Notice that since the first two modes are required to implement and considered as main operating modes and the others are optional, the discussion of platform will be located on the second modes hereinafter.

In the specification of IEEE 802.11g, it stats that the transmit center frequency tolerance shall be ±25 ppm maximum [3]. If we consider the receiver, the maximum relative frequency between the transmitter and the receiver is confined to ±50 ppm. Hence, the maximum frequency offset is ±120 kHz with 2.4 GHz carrier frequency.

The symbol clock frequency tolerance is also defined in the standard. The transmit center frequency and symbol clock frequency shall be derived from the same reference oscillator. This means that the error in ppm for the carrier and the symbol timing shall be the same [3]. The clock frequency offset between the transmitter and the receiver shall be ±25 ppm maximum, that is, ±0.8 kHz with a fundamental sample rate of 20 MHz.
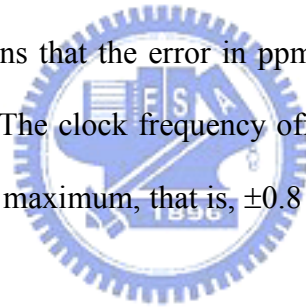
2.2 System Block Diagram

The following three sections comprise of transmitter, channel model and receiver are the main parts in our simulation platform. Transmitter combines OFDM and DSSS systems. Next are the channel model introduction and the signal modeling. In the end is the universal receiver which share hardware of two modes. Two important blocks, automatic frequency control (AFC) and phase recovery (PR), will be presented for total system integration.

2.2.1 Transmitter

Figure 2.4 is the transmitter block diagram. After the parameters of data rate and data length are decided, following the blocks one by one will generate the transmitted signals, and the MUX that depends on operation mode will select the signal that be sent to air by antenna after up-conversion the baseband signals to operating channel frequency.
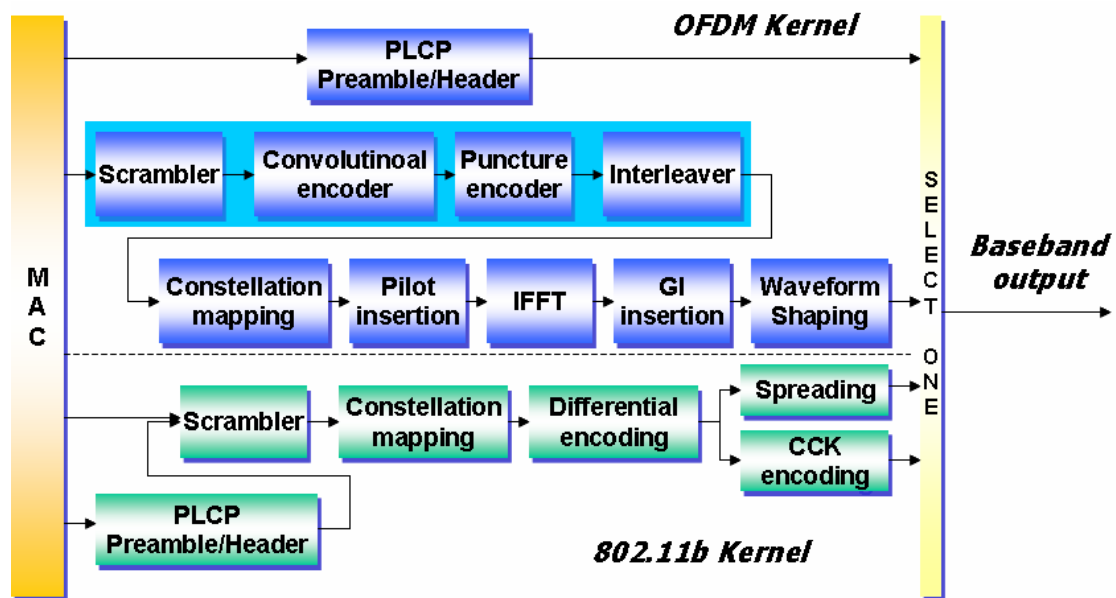
Figure 2.4 Block diagram of transmitter.

2.2.2 Channel Model

AWGN, multipath, carrier frequency offset, phase noise and sampling clock offset are simulated in the channel, where the AWGN is added, the multipath is convoluted, CFO which joint phase noise is multiplied and SCO is convoluted with *sinc* wave to the Tx signal. The parameter of the AWGN channel is the signal-to-noise ratio (SNR) in dB, and for CFO and SCO is the frequency offset in ppm proportional to the carrier

frequency and the symbol sampling frequency respectively. As for the multipath fading channel, the parameters include the channel type, the root-mean-square (rms) delay spread value and the tap numbers. The loop bandwidth and the loop time constant of the low-pass filter in phase-locked loop (PLL) decide the range of phase noise. Figure 2.5 shows the practical and the baseband equivalent channel model.
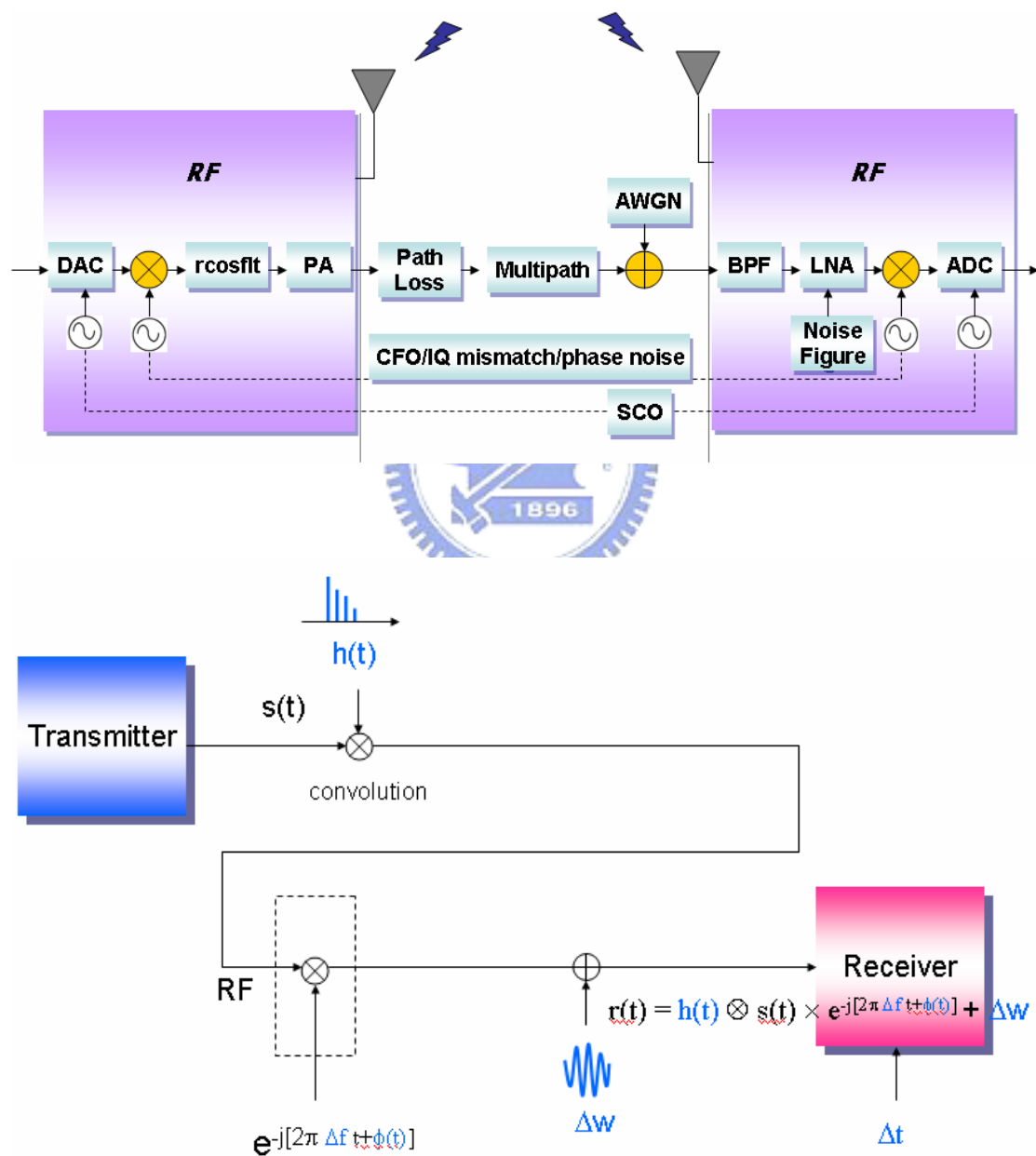
Figure 2.5 Channel model and the baseband equivalent channel model.

2.2.2.1 AWGN

In communications, the additive white Gaussian noise (AWGN) channel model is one in which the only impairment is the linear addition of wideband or white noise with a constant spectral density (expressed as W/Hz of bandwidth) and a Gaussian distribution of amplitude. The model does not account for the phenomena of fading, frequency selectivity, interference, nonlinearity or dispersion. However, it produces simple, tractable mathematical models which are useful for gaining insight into the underlying behavior of a system before these other phenomena are considered.

Wideband Gaussian noise comes from many natural sources, such as the thermal vibrations of atoms in antennas, "black body" radiation from the earth and other warm objects, and from celestial sources such as the sun.

The AWGN channel is a good model for many satellite and deep space communication links. On the other hand, it is not a good model for most terrestrial links because of multipath, terrain blocking, interference, etc.

The signal distorted by AWGN can be derived as

$$r(t) = s(t) + n(t) \tag{2.1}$$

In equation (2.1), s(t), r(t), n(t) stand for the transmitted, received signal and AWGN respectively. It causes the received signal fluctuated. This effect is illustrated in Figure 2.6. Other channel effects become more severely when AWGN joins without any compensation. A common solution but not the panacea, moving average, can just mitigate this symptom.
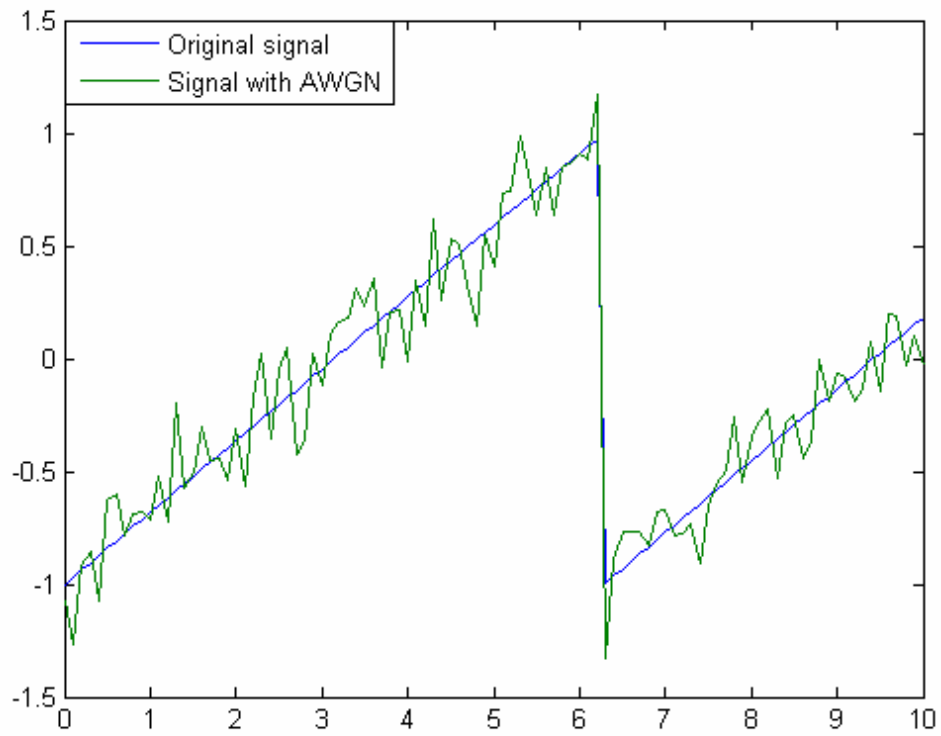
Figure 2.6 The received signal with and without AWGN.
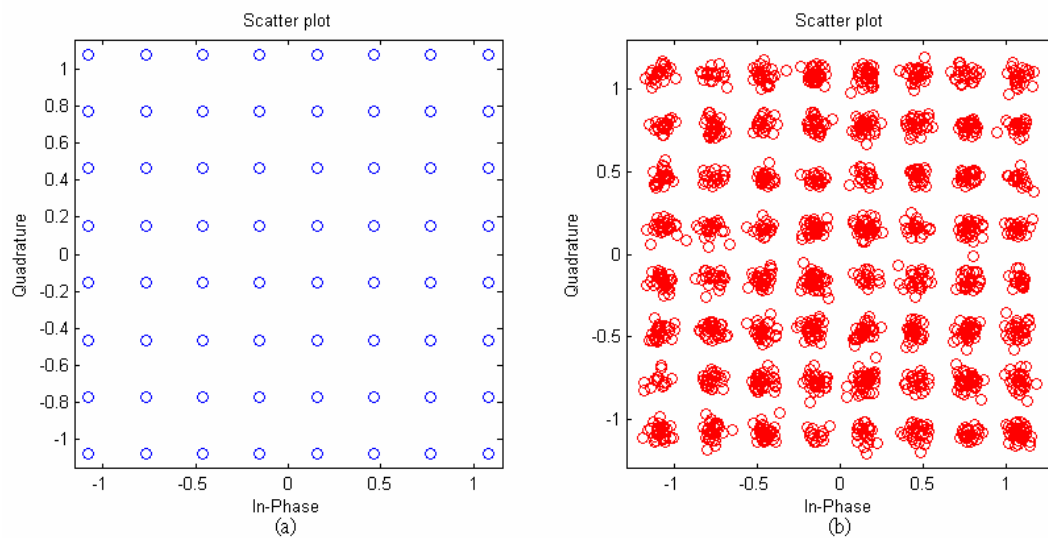
Figure 2.7 The signal constellation after FFT output.

(a) Original signal. (b) Signal with AWGN.

11

2.2.2.2 Multipath

Communication signal is transmitted through the air to a receiver. That signal will likely take several different paths before it reaches the receiver. Besides the direct path there are reflected path and scattering signal. The propagation phenomenon is called multipath in telecommunication. And it usually goes alone with severe fading results in a signal reduction of more than 30dB. All of these signal paths are combined at the receiver to produce a signal that is a distorted version of the transmitted signal. Multi-path is usually described by two sorts:

A.   Line-of-sight (LOS): the direct connection between the transmitter (TX) and the receiver (RX).

B.   Non-line-of-sight (NLOS): the path arriving after reflection from reflectors.

Figure 2.8 shows the origin of multipath and the corresponding effect in communications. The effects of multipath include constructive and destructive interference, and phase shifting of the signal. This causes Rayleigh fading, named after Lord Rayleigh. The standard statistical model of this gives a distribution known as the Rayleigh distribution. Rayleigh fading with a strong line of sight content is said to have a Rician distribution, or to be Rician fading. In high speed WLAN for indoor environment, multipath can cause errors and affect the quality of communications. The errors are due to inter-symbol interference (ISI) and frequency-selective fading when the maximum delay spread of the channel is larger than symbol period or channel coherent bandwidth is smaller than data bandwidth. In IEEE 802.11g application, the receiver design must guarantee the performance under the multipath fading channel with maximum delay spread smaller than guard interval (GI) of OFDM symbol.
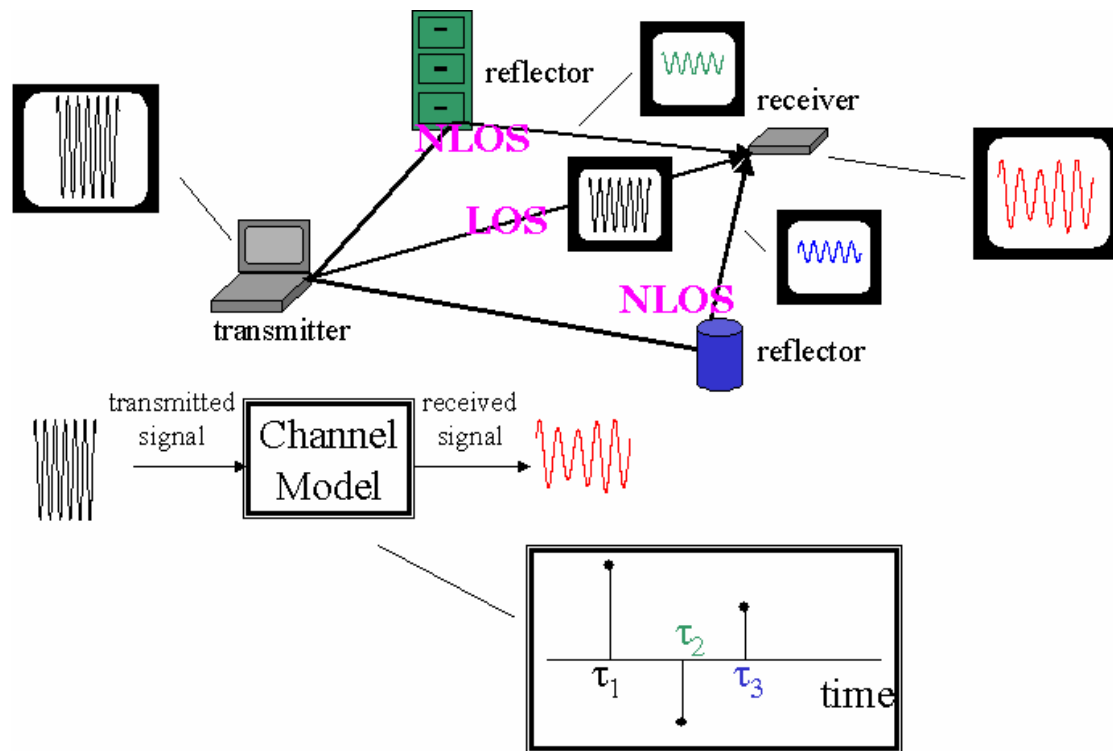
Figure 2.8 Multipath: origin and phenomena.

In our MATLAB platform, we use two kinds of multipath fading channel models. One is the power decay exponential (PDE) model. The model is extracted from SPW multipath channel model. It has exponentially decaying power and random uniformly distributed phase. Another is the IEEE channel model specified by IEEE 802.11 working group. It has Rayleigh distributed magnitude with average power decaying exponentially and random uniformly distributed phase. We use the later typically in the simulation. Figure 2.9 shows the impulse response and frequency response of an IEEE channel with 50 ns rms delay spread.
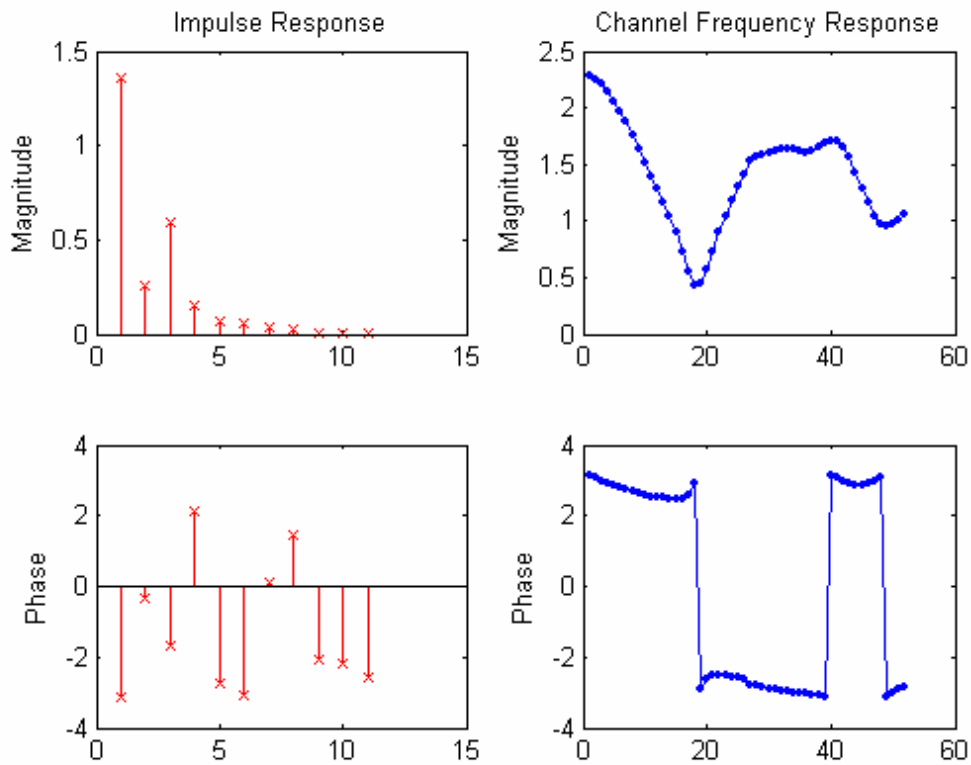
Figure 2.9 An impulse response and frequency response of IEEE channel.

We can include the channel effects to form a specific channel model, and do a convolution with transmitted signal to form the received signal output. The signal through the multipath fading channel in time and frequency domain would be

$$r(t) = s(t) \otimes h(t) \tag{2.2}$$

$$Y(f) = X(f) \cdot H(f) \tag{2.3}$$

where h(t) is channel impulse response (CIR) and H(f) is channel frequency response (CFR). As mentioned before, ISI would be the biggest problem if we do nothing against the multipath. Equalizers are often used to correct the ISI. Before OFDM technique rising, the conventional equalizers, adaptive time domain equalizer (TDE),

widespread in the world. But frequency domain equalizer (FDE) or hybrid mechanisms become more popular now. FDE has good properties like faster convergence and more simple mathematical derivation than TDE although it needs higher hardware complexity.

In the mobile communication consideration, IEEE 802.11g is the WLAN application for indoor environment with maximum Doppler frequency of 50 Hz. So the coherent time of channel is 20 ms. In the packet-based transmission, the maximum packet slot is about 1.2 ms (6 Mbits/s mode). Because one packet slot is a lot smaller than coherent time, we can consider the channel as the slow fading channel and is almost static [4]. We find the Doppler Effect just rotates the end signal of a packet by 0.3 radians from the simulation.

2.2.2.3 CFO
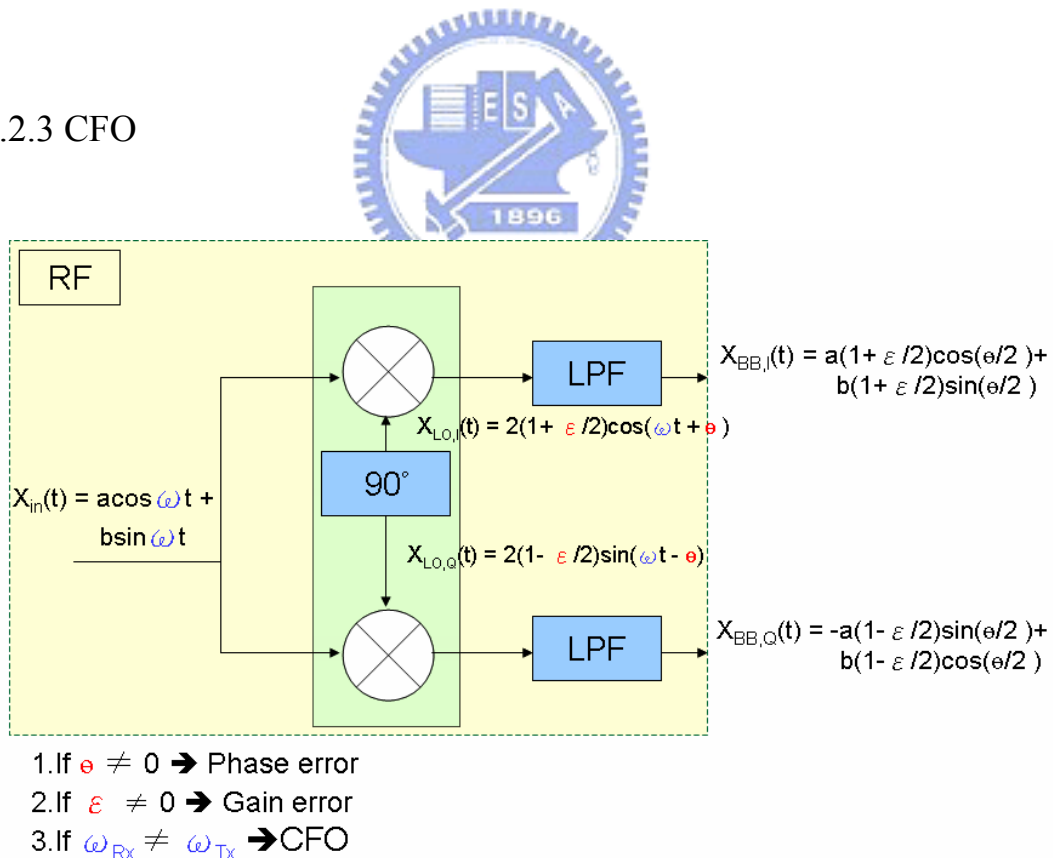
Figure 2.10 The whys and wherefores of CFO and I/Q mismatch.

In the RF front-end, CFO exists between the transmitter and the receiver. The signal distortion with CFO can be derived as

$$r(t) = \frac{1}{T} \int_0^T \cos(2\pi ft + m(t)) e^{-j2\pi(f+\Delta f)t} = e^{m(t)} \cdot e^{-j2\pi\Delta ft} = s(t) \cdot e^{-j2\pi\Delta ft} \qquad (2.4)$$

In equation (2.4), r(t) is the received signal; $\cos(2\pi ft+m(t))$ is the passband transmitted signal; $e^{-j2\pi(f+\Delta f)t}$ is the passband receiver with CFO Δf; $e^{m(t)}$ is baseband transmitted signal. We find CFO will rotate the received signal with a linear phase of $-2\pi\Delta ft$. In frequency domain, the intercarrier interference (ICI) will occur due to the linear phase error in time domain. When CFO is smaller than ± 2 ppm of 2.4 GHz, ICI phase error is not obvious since the frequency shift (< 1/3 subcarrier space) is small. Then the linear shift of mean phase will be apparent in frequency domain [4].Once CFO occurs, the constellation would rotate continuously, and cause the packet error rate (PER) keeps high even when SNR increases.
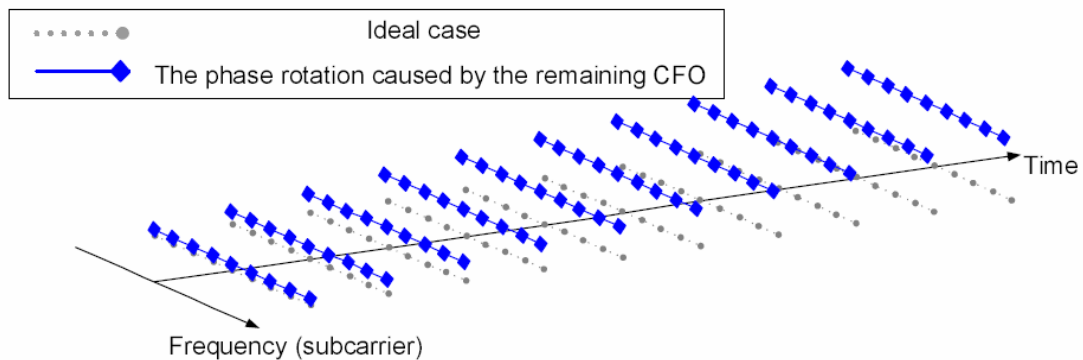
Figure 2.11 The symbol rotation angle is increasing with time.

AFC is the most common circuit that maintains the frequency of an oscillator within the specified limits with respect to a reference frequency. With this powerful

device, we can easily compensate our performance loss due to CFO.

2.2.2.4 Phase Noise

In an oscillator, phase noise is rapid, short-term, random fluctuations in the phase of a wave, caused by time domain instabilities. The performance of synchronization tracking loops depends strongly on the phase noise characteristics. Phase noise, $L(f)$ in decibels relative to carrier power (dBc) on a 1 Hz bandwidth, is given by:

$$L(f) = 10\log\left[0.5S_\varphi(f)\right] \tag{2.5}$$

where $S_\varphi(f)$ is the spectral density of phase fluctuations.
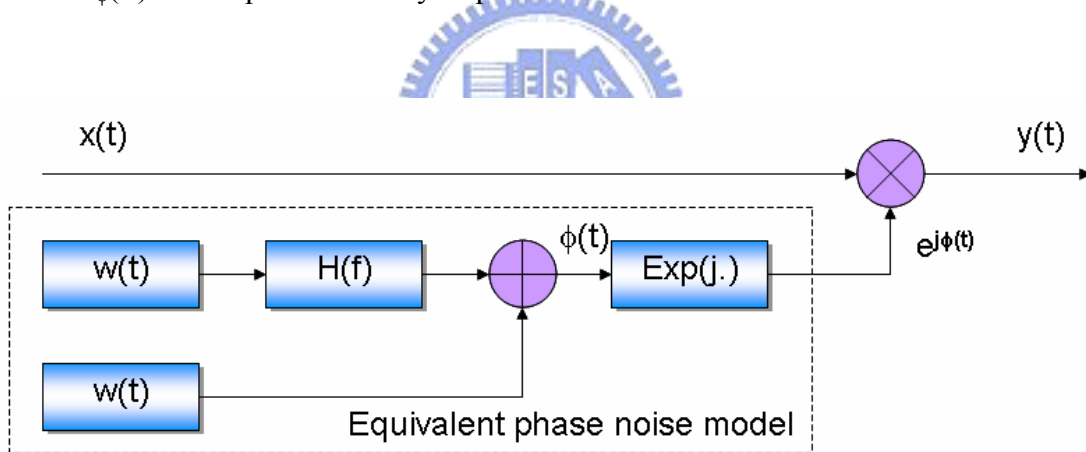
Figure 2.12 Measurement based power density spectrum phase noise model.

Various phase noise models exist for the analysis of phase noise effects. An often used model which assumes instability of the phase only is described in the following [18].

$$H(f) = 10^{-c} + \begin{cases} 10^{-a} & |f| \le f_1 \\ 10^{b(f_1-f)/(f_2-f_1)-a} & f > f_1 \\ 10^{b(f_1+f)/(f_2-f_1)-a} & f < -f_1 \end{cases} \tag{2.6}$$

Measurement based power density spectrum is an approach used within the standardization of DVB-T. The parameters a and f_1 characterize the phase lock loop and the parameter c the noise floor. The steepness of the linear slope is given by b and the frequency f_2 indicates where the noise floor becomes dominant. A plot of the power density spectrum with typical parameters is shown Figure 2.13. This phase noise process can be modeled using two Gaussian noise processes. The first noise term is filtered by an analog filter with a transfer function as shown above, while the second term gives a phase noise floor which depends on the tuner technology.
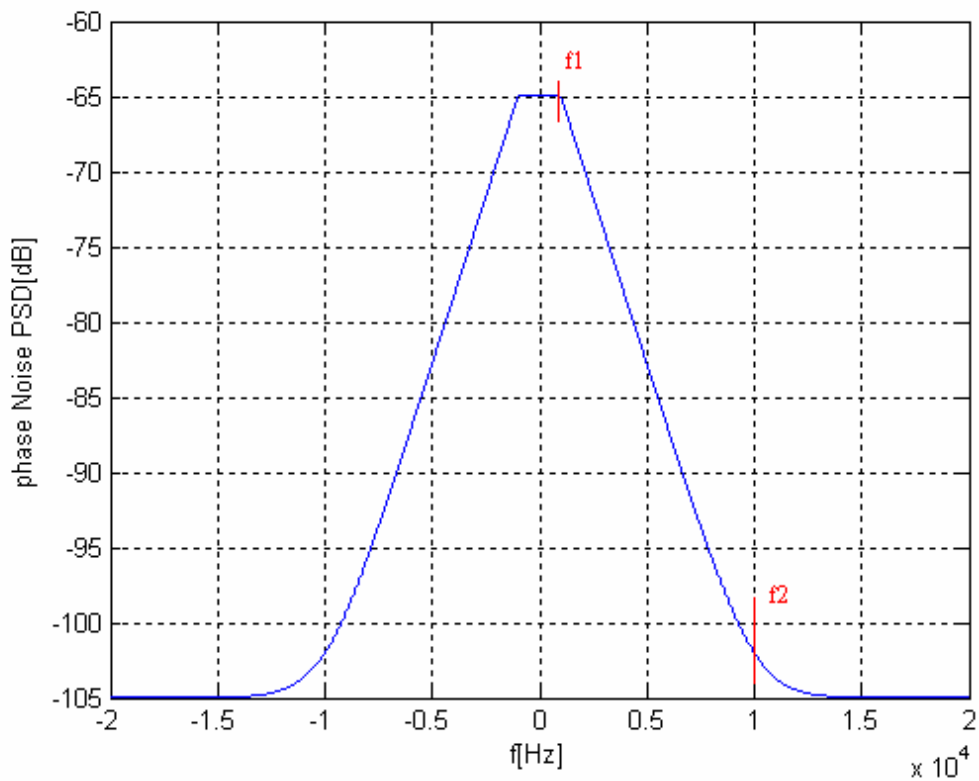
Figure 2.13 Phase noise power density spectrum.

For brevity but without loss of generality, it is assumed that the transmitted signal is only affected by phase noise $\varphi_N(t)$. The oscillator output and the signal at the FFT

output corresponding to subcarrier n are given by

$$r(t) = s(t)e^{j\varphi_N(t)} \tag{2.7}$$

$$R_n = S_n I_0 + \sum_{\substack{m=0 \\ m \neq n}}^{N_c-1} S_m I_{n-m} \text{ where } I_n = \frac{1}{T_s} \int_0^{T_s} e^{j2\pi f_n t} e^{j\varphi_N(t)} dt \tag{2.8}$$

According to equation, the effects of phase noise can be separated into two parts. The component I_0 in the first term represents a common phase error due to phase noise which is independent of the subcarrier index and is common to all subcarriers. The sum of the contributions from the N_c-1 subcarriers given by the second term represents the ICI caused by phase noise. The ICI depends on the data and channel coefficients of all different N_c-1 sub-channels such that the ICI can be considered as Gaussian noise for large N_c.

In practical, CFO and phase noise are jointly occur and severely degrade the system performance. And considering the PLL converging tendency, we can find that the phase is vibrating in some range instead of looping to a value after PLL converged. This behavior looks like a sin wave, so we construct a CFO joint phase noise model in the following way for brevity but without loss of generality.

$$2\pi\Delta f t + \varphi_N(t) = 2\pi\Delta f t + B \cdot \sin(\Delta w t) + n(t) \tag{2.9}$$

where B stands for loop bandwidth of the low pass filter (LPF) in PLL, decides the magnitude. And $\Delta\omega$ is the loop time constant which in charge of the swing period. n(t) is the high frequency noise. The proposed model can totally equivalent the previous model but is more practical.

If we can't precisely acquire the CFO value, there's remaining effects hereafter.

Hence, we may need a phase noise detector for eliminating the phase noise
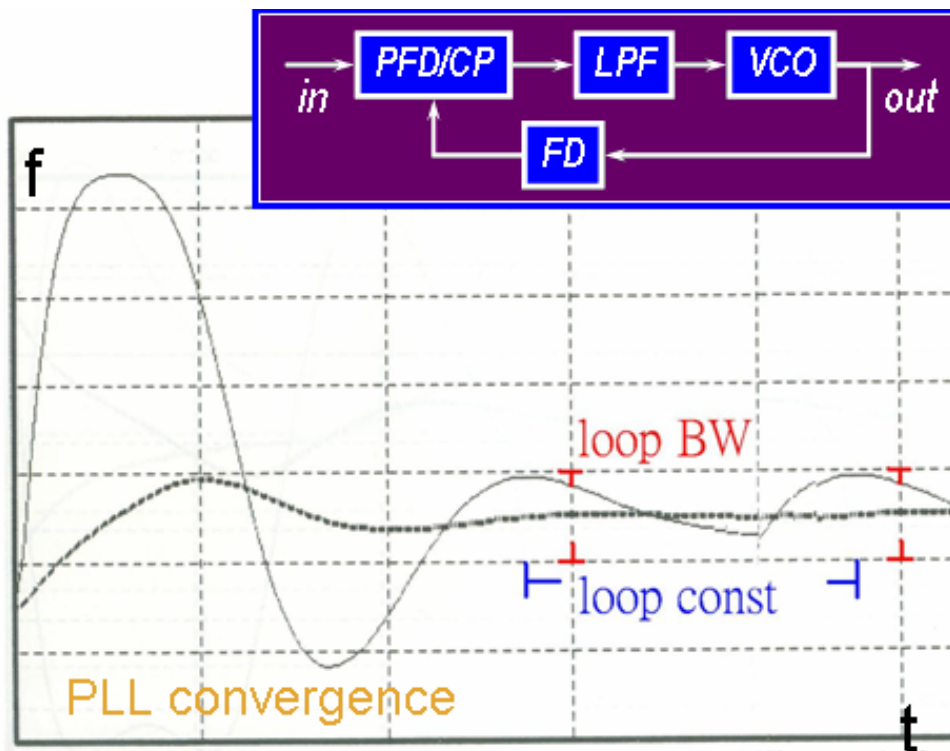
Figure 2.14 PLL converging tendency.
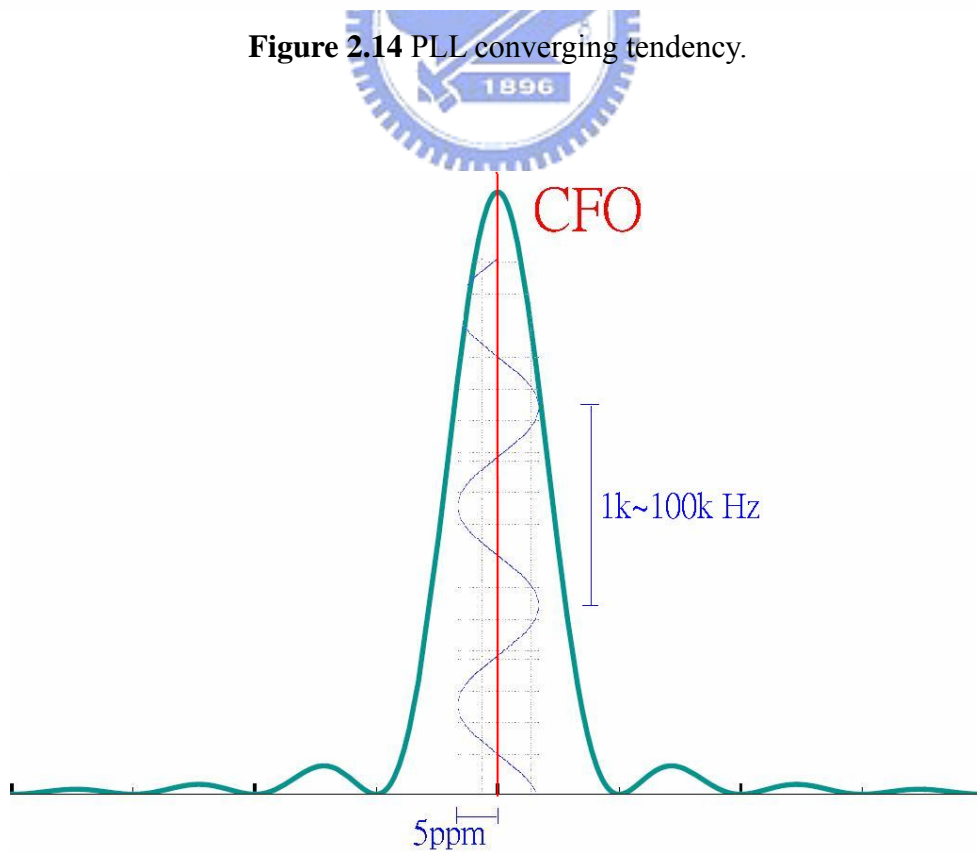
Figure 2.15 Characteristic of carrier frequency statistics.

2.2.2.5 SCO

The interfaces of RF and baseband data are digital to analog converter (DAC) in the transmitter and analog to digital converter (ADC) in the receiver side. The oscillators used to generate the DAC and ADC sampling instants at the transmitter and receiver will never have exactly the same period. The ADC is the first stage of baseband, so it dominates the receiving SNR. To get the highest input SNR, the ADC is hoped to sample at the eye open position where it has the maximum signal power. However, the initial sampling phase could be anywhere in the eye diagram, so timing synchronization is necessary. The ADC has two kinds of clock source: free running clock and PLL output clock. With free running clock, this method also called non-synchronous sampling or fix sampling, clock frequency and phase are fixed. Once timing error estimated, the compensation would be performed with interpolator. With PLL output clock, also called synchronous sampling or dynamic sampling, it receives the timing error and adjusts its frequency and phase to compensate the error. There is a need to maintain synchronization while the accuracy and stability of the original clock reference in the receiver may not be ideal. These tasks are the responsibility of a specific module Delay Lock Loop (DLL). Figure 2.16 shows an example of oversampled signal with SCO.
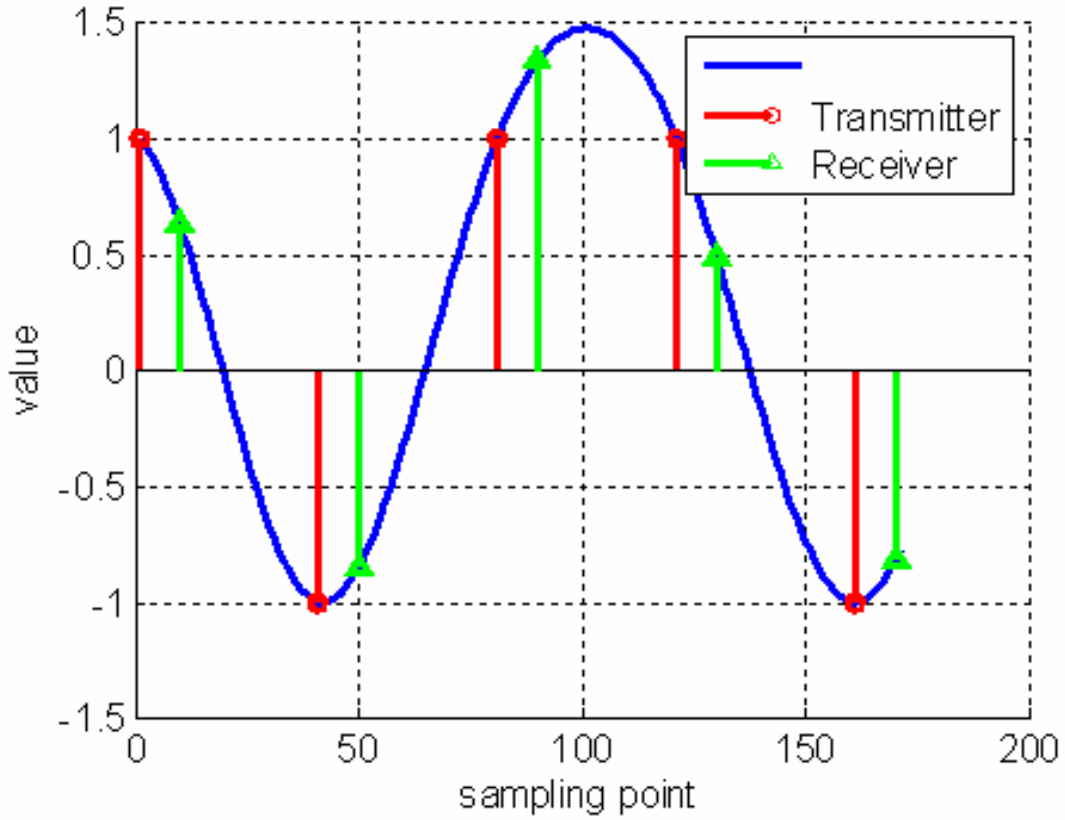
Figure 2.16 An example of oversampled signal with SCO.

In the MATLAB platform, the model of clock drift is built using the concept of interpolation. The input digital signal and the shifted *sinc* wave can interpolate the value between two sampling points. The sampling phase can be written as $nT_S - \Delta P_N$. And then we get the ADC output signal $R(nT_S)$ by convoluting the ADC input signal $R_{preADC}(nT_S)$ and shifted *sinc* wave. The received signal after ADC can be derived as equation where (2.10) l is the sampling point index.

$$R(nT_S) = R_{preADC}(nT_S) \otimes \sin c(\frac{nT_S - \Delta P_n}{T_S})$$
$$= \sum_{k=-l}^{l} R_{preADC}(nT_S - kT_S) \cdot \sin c(k - \frac{\Delta P_n}{T_S})$$

(2.10)

SCO brings a slow shift of the symbol timing point, which rotates subcarriers. And a loss of SNR due to ICI generated by the slightly incorrect sampling instants. The shift of sampled phase in time domain will induce the linear phase error in frequency domain. Figure 3.x shows the frequency domain behavior of SCO model in the system platform. When clock cycle increases, the range of linear phase error will increase.
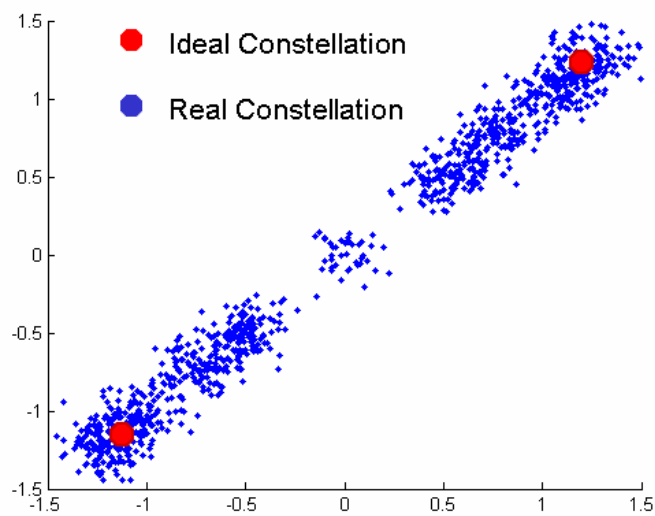
Figure 2.17 Clock drift makes constellation dispersed.
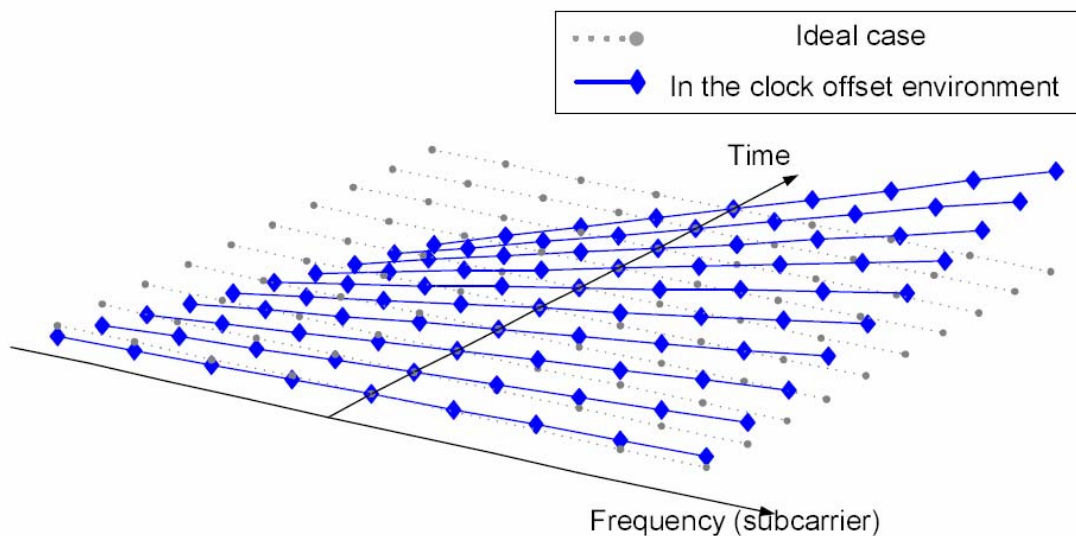
Figure 2.18 The phase rotation on each subcarrier under SCO environment.

23

2.2.3 Receiver

Figure 2.x shows the block diagram of the receiver. The data path for OFDM data occupies much more hardware resource than that for DSSS/CCK ones. The overall AFC mechanism can almost be combined together. DSSS/CCK takes advantage of match-filter output for CFO estimation. Phase recovery compensates the mean phase error due to residuary CFO and linear phase error due to clock offset. It uses pilots to detect the shift of subcarriers in frequency domain. Match filter is used to get peak with Barker correlation in 11b. Then CFO estimator will calculate CFO roughly with correlation results. Besides, it also deals with the phase synchronization and CFO tracking of 11b.
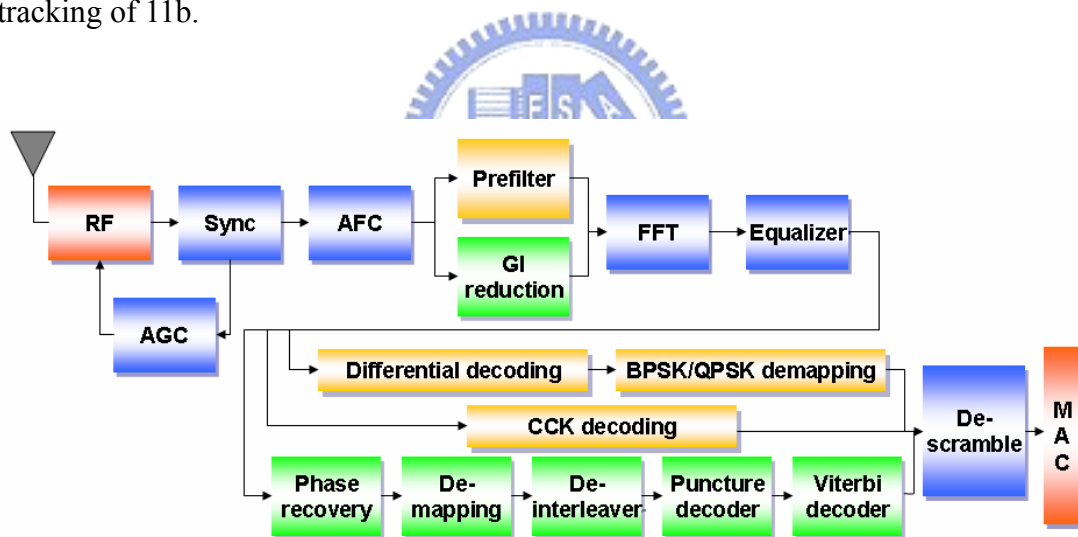
Figure 2.19 IEEE 802.11g receiver baseband diagram.

2.2.3.1 Related Work of CFO

The CFO master, Moose, proposed a CFO estimation method which uses period property of preamble in 1994. When receiving two repeat training symbols, all subcarriers in the first symbol will rotate a same angle to the same subcarriers in the second symbol if CFO occurs. The rotate angle is the integration of the frequency

offset.

In equation (2.11), r_n is the received training symbol interfered by CFO, ε, and $-K \sim K$ are subcarriers' indexes.

$$r_n = \frac{1}{N} \sum_{k=-K}^{K} X_k H_k e^{j2\pi(k+\varepsilon)n/N} \text{ where } n = 0,1,...,2N-1 \qquad (2.11)$$

$$R_{1k} = \sum_{n=0}^{N-1} r_n e^{-j2\pi nk/N} \qquad (2.12)$$

$$R_{2k} = \sum_{n=N}^{2N-1} r_n e^{-j2\pi nk/N} = \sum_{n=0}^{N-1} r_{n+N} e^{-j2\pi nk/N} \qquad (2.13)$$

From equation (2.11), we know that $r_{n+N} = r_n e^{j2\pi\varepsilon}$, and R_{2k} becomes (2.14)

$$R_{2k} = \sum_{n=0}^{N-1} r_n e^{-j2\pi\varepsilon} e^{-j2\pi nk/N} = e^{-j2\pi\varepsilon} R_{1k} \qquad (2.14)$$

That means there exits a phase rotation between the first symbol and the second one. When receiving, the CFO can be estimated from the received repeat OFDM symbols.

$$\hat{\varepsilon} = \frac{1}{2\pi} \tan^{-1} \left\{ \frac{\sum_{k=-K}^{K} \text{Im}\left[R_{2k} R_{1k}^{*}\right]}{\sum_{k=-K}^{K} \text{Re}\left[R_{2k} R_{1k}^{*}\right]} \right\} \qquad (2.15)$$

This algorithm, however, can only correctly distinguish the phase rotation in the range between -π and π. The estimation limitation is shown in equation (2.16). In (2.16) and (2.17), the NT_S means the time interval between the two repeat symbols. Minimizing the interval time to the OFDM symbol time can make the maximum CFO estimation range to be half of the subchannel bandwidth. According to equation (2.17), the method to get a larger CFO estimation range is to shorten the training symbol time

[19].

$$|2\pi\varepsilon| = |2\pi NT_S \Delta f| < \pi \tag{2.16}$$

$$|\Delta f| < \frac{1}{2NT_S} \tag{2.17}$$

2.2.3.2 CFO Estimation and Compensation

In packet-based transmission system, training symbols are provided for burst synchronization. From previous discussion in section 2.2.3.1, the repeat OFDM symbols can be used to perform the CFO synchronization. It can also be used to do the frame detection and be the equalizer training data. Using the Moose's algorithm, however, the CFO is estimated after the FFT. In order to provide more reliable information to the frame detector and equalizer, the training data have to be retransformed after compensating the CFO. Unfortunately, this is not allowed in time space.

Based on the above issues, we suggest that the time domain CFO estimation is more suitable for WLAN system than the frequency domain approach. The equation (2.19) is the time domain estimation. The equation of the maximum estimation range is same with that of the frequency domain estimation.

$$z = \sum_{n=0}^{D-1} r_{n+D} \cdot r_n^* = \sum_{n=0}^{D-1} r_n e^{j2\pi\varepsilon} \cdot r_n^* = e^{j2\pi\varepsilon} \sum_{n=0}^{D-1} |r_n|^2 = e^{j2\pi\Delta f DT_S} \sum_{n=0}^{D-1} |r_n|^2 \tag{2.18}$$

$$\Delta f = \frac{1}{2\pi DT} \tan^{-1} z = \frac{1}{2\pi DT_S} \tan^{-1} \left\{ \frac{\operatorname{Im} \sum_{n=0}^{D-1} r_{n+D} \cdot r_n^*}{\operatorname{Re} \sum_{n=0}^{D-1} r_{n+D} \cdot r_n^*} \right\} \tag{2.19}$$

Using time domain estimation and compensation, the CFO is estimated and

training pattern is compensated before the FFT transformation. One advantage is that the frame detector can get a clearer training pattern to judge the frame boundary more accurately. The other advantage is that the compensated training data can be used to estimate the channel response directly by the equalizer.

In order to cover a larger CFO estimation range, two-stage CFO estimator is needed. First is the coarse CFO estimation and compensation using two short repeat training symbols and then the fine synchronization is performed by using two long training symbols.
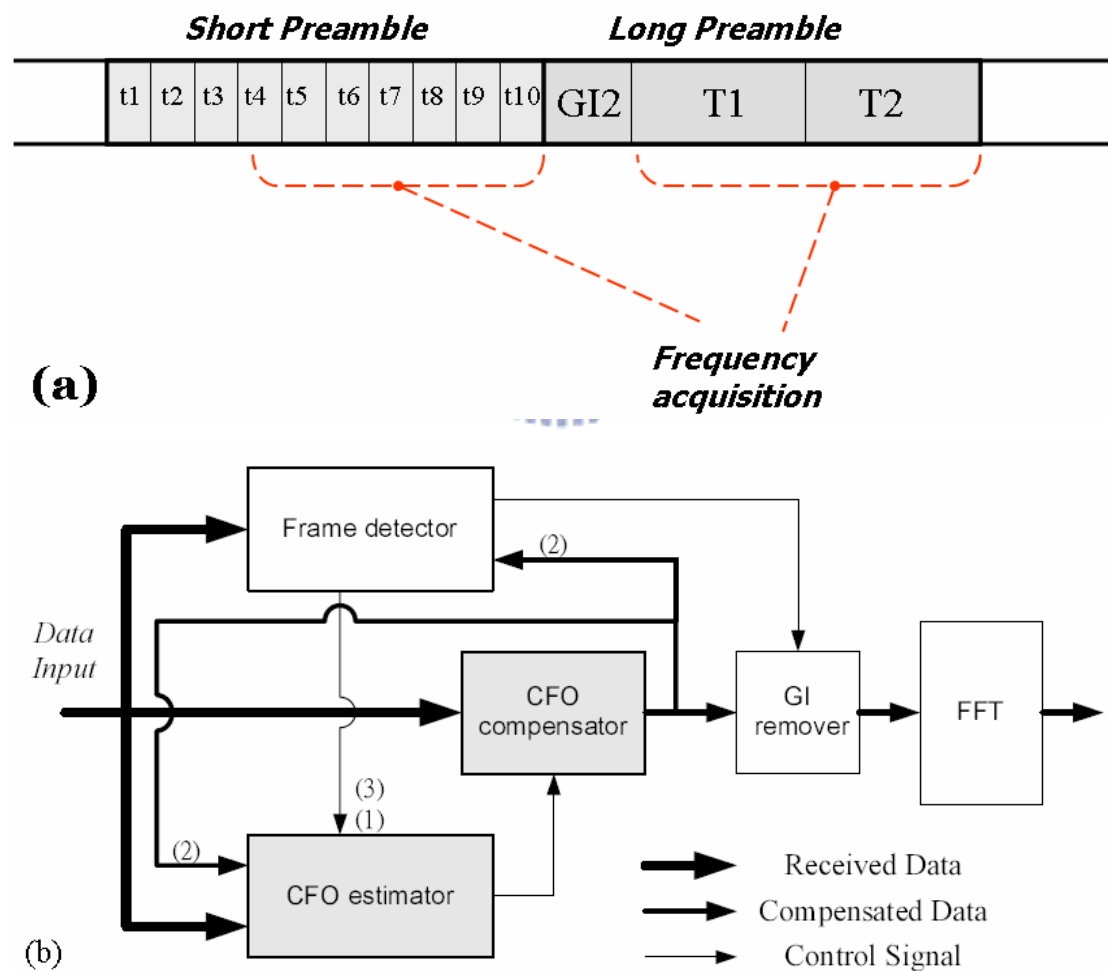
Figure 2.20 (a) The training pattern. (b) CFO synchronization structure and interaction between frame detector and CFO compensator.

In our design, coarse and fine CFO estimations and compensations are performed by using the same algorithm and there is no overlap time in the flow. We can use only one estimator and a compensator to achieve these two jobs. Following, the synchronization flow and the interactive between the frame detection and CFO compensation will be explained using Figure 2.20 and Figure 2.21.

The frame detector is always working for detecting the short training sequence. After it detects short training symbols, the CFO estimator is noticed to start working by the control signal (1) in Figure 3.20. The CFO estimator uses the short training symbols to estimate the coarse CFO. Then the compensator starts to compensate the following received data. It inputs the compensated data into the frame detector and the CFO estimator from datapath (2). The frame detector and CFO estimator are working at the same time. Once the long training sequence is detected, the frame detector will send information to the GI remover and the CFO estimator with the control signal (3) to declare the frame boundary. Then the estimator can calculate the fine CFO immediately. After the frame boundary and fine CFO are estimated, the frame detector and estimator will be turned off. The remaining transmission data after the long training sequence must be compensated with the total estimated CFO. One by one the GI will be removed and then OFDM symbol will be inputted into the FFT after CFO compensation. The pre-FFT synchronization is finished. The CFO compensator and the GI remover are the two function blocks still have to work continuously.
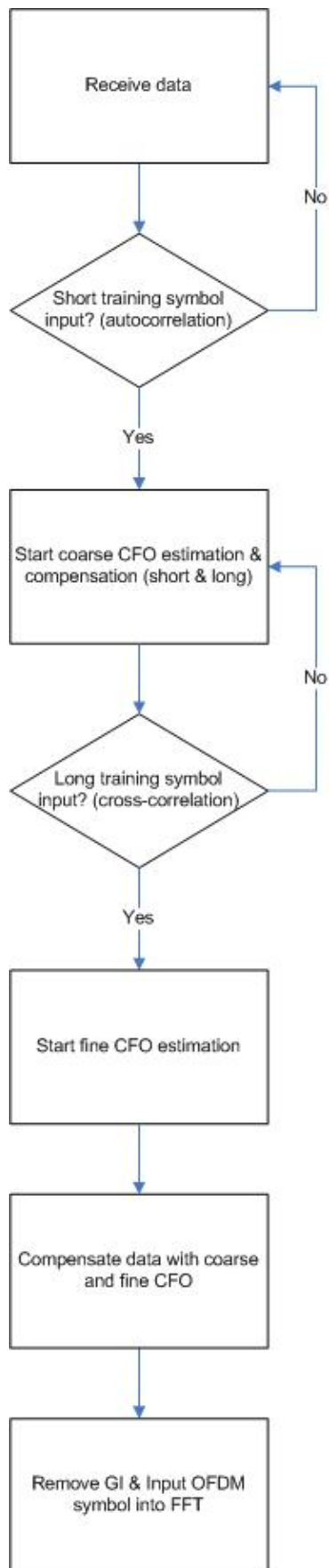
Figure 2.21 The pre-FFT synchronization flowchart.

Because of the influence of channel and other effect, the estimation and compensation of CFO is not perfect. The residual CFO will still affect the received data .ICI is the one of effects from the remaining CFO. Equation (2.20) and (2.21) are the compensated data sequence and transformed frequency domain data.

$$y_n = x_n e^{-j2\pi n T_S (\Delta f - \widehat{\Delta f})} \tag{2.20}$$

$$
\begin{aligned}
Y_{lk} &= \sum_{n=0}^{N-1} y_{lN_G + n} e^{-j2\pi kn/N} \\
&= \sum_{n=0}^{N-1} x_{lN_G + n} e^{-j2\pi (lN_G + n) T_S (\Delta f - \widehat{\Delta f})} \cdot e^{-j2\pi kn/N} \\
&= e^{-j2\pi lN_G T_S (\Delta f - \widehat{\Delta f})} \sum_{n=0}^{N-1} x_{lN_G + n} e^{-j2\pi n T_S (\Delta f - \widehat{\Delta f})} \cdot e^{-j2\pi kn/N} \\
&= e^{-j2\pi lN_G T_S (\Delta f - \widehat{\Delta f})} \cdot (X_{lk} + N_{ICI}(l,k))
\end{aligned}
\tag{2.21}
$$

If the ICI in equation (2.21) is small enough (< 1ppm), it can be view as complex zero-mean Gaussian noise and usually can be ignored.

2.2.3.3 Phase Recovery

In our proposed synchronization method, the remaining CFO and SCO compensation are solved at the same time in the frequency domain. Because the estimation and compensation method are all performed by estimating and compensating the data phase, this partition can be called as "Post-FFT Phase Compensator".

According to the equation (2.21) and (2.x), the remaining CFO and SCO will present some symptoms at the carrier phase. However, there are some different between the two effect. From equation (2.21), we know that the remaining CFO will induce a phase rotation to all the carriers in an OFDM symbol. The SCO will induce a linear phase rotation shown in the equation (2.x). The jointed effect of the two offsets

is shown in Figure 2.22. Here we will propose a compensation method which can mitigate these two effects. We compensate the two effects at the same time in frequency domain and the signal upsampling and feedback to time domain control are not needed.
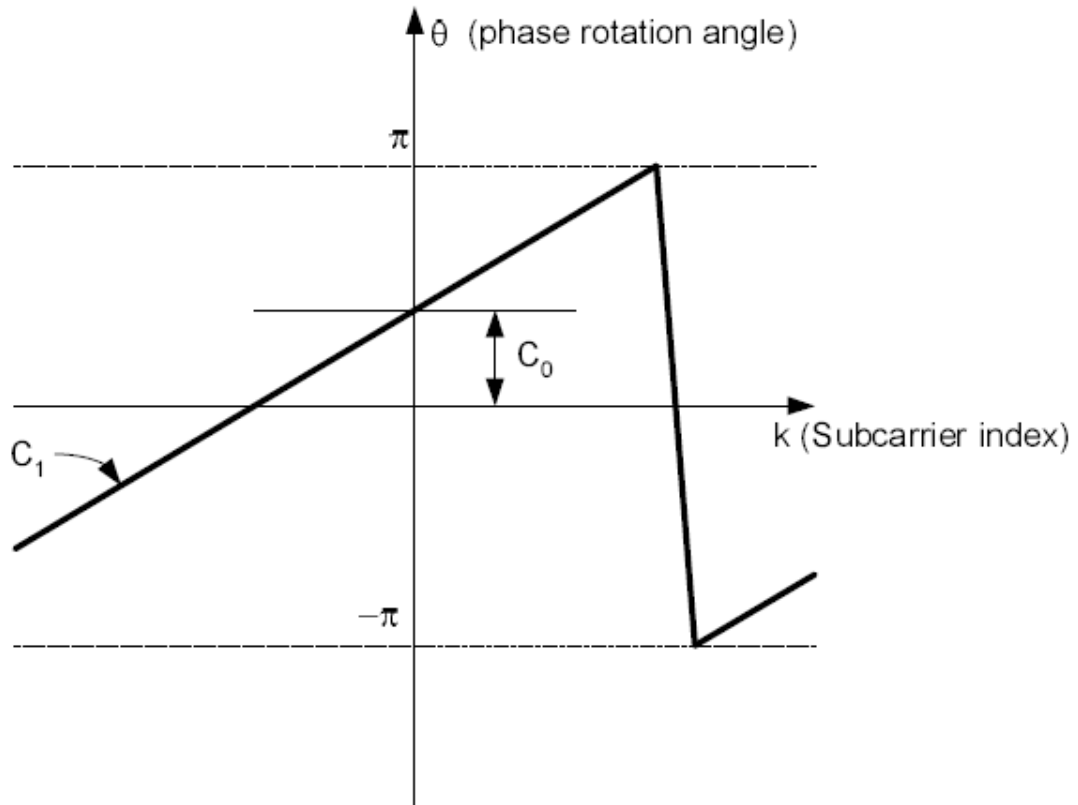
Figure 2.22 Phase rotation of each subcarriers in an OFDM symbol.

From above figure, the behavior of the carrier phase suffered from effect of the remaining CFO and SCO can be modeled as a linear equation (2.22). The k means the subcarrier's indexes, the $\theta_{l,k}$ is the phase rotation of the l_{th} symbol k_{th} carrier and C_{0l}, C_{1l} are two coefficients.

$$\theta_{l,k} = C_{0l} + C_{1l}k \tag{2.22}$$

$$C_0 = \frac{1}{M}\sum_k \theta_k \tag{2.23}$$

$$C_1 = \frac{\sum_k k \cdot \theta_k}{\sum_k k^2}$$

(2.24)

The problem of the remaining CFO and SCO is that the phase distortion will cause decision error if the rotation angle is larger than the decision boundary. The most direct compensation method is to compensation the rotation angle with the opposite direction directly. Each subcarrier's rotation angle can be calculated using the equation (2.22). And the least squares algorithm is used to estimate these two coefficients. The angle of the pilot data can be used to perform the estimation. Because of channel noise and ICI, some estimation results are not very stable. In our design, weighting function and moving average are needed for a more stable compensation. Figure 2.23 is the phase recovery block diagram.
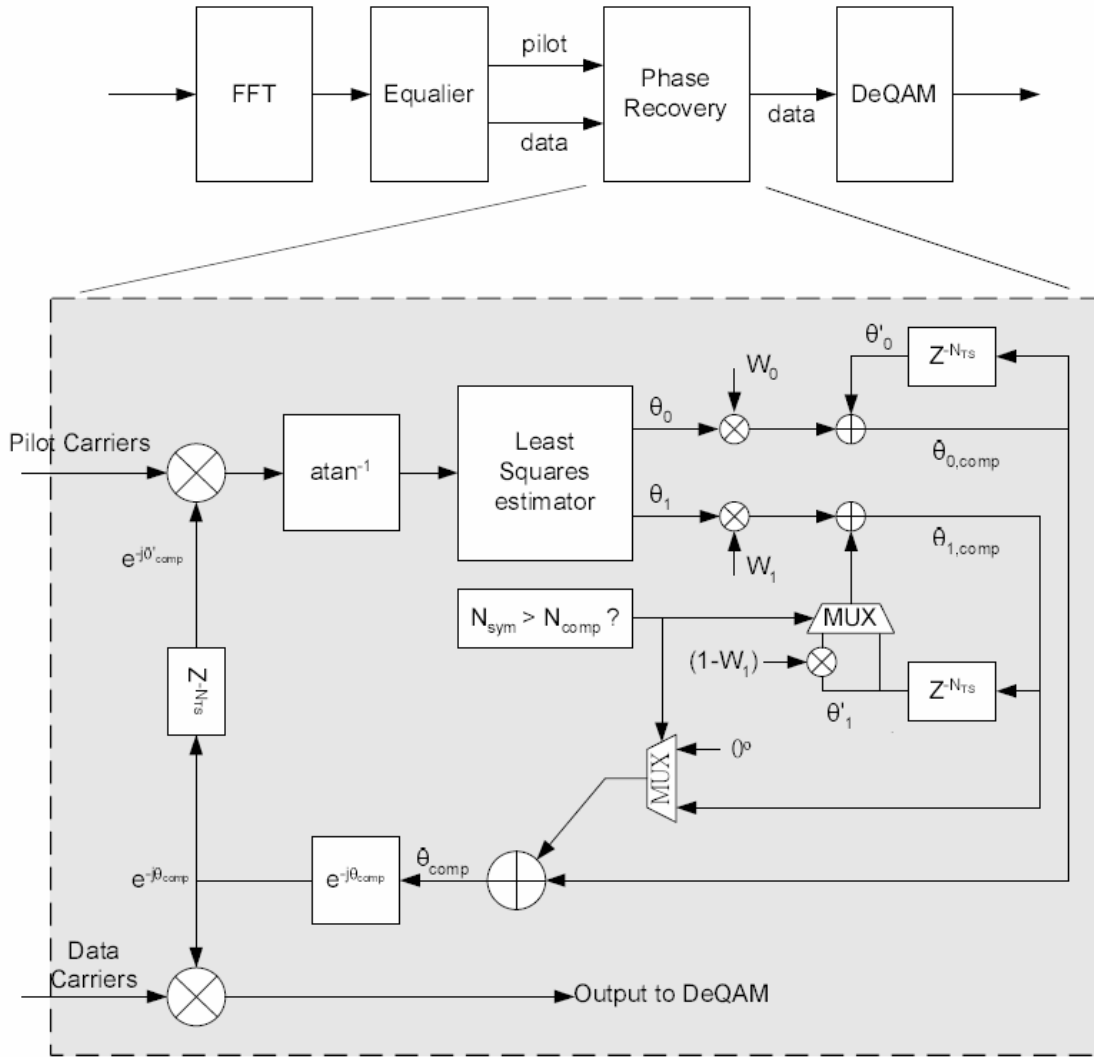
Figure 2.23 The phase recovery block diagram.

The θ_0 is equal to the mean phase term C_0 in equation (2.22). The θ_1 is the linear phase term which is equal to the $C_1 \cdot k$. The $\theta_{0,comp}$ and $\theta_{1,comp}$ are the estimation phase having to be compensated to each subcarrier. The $\theta_0{}'$ and $\theta_1{}'$ are the estimation phase of the last symbol. W_0 and W_1 are weighting coefficients for the θ_0 and θ_1. N_{TS} is the OFDM symbol time including GI.

Because the pilot phase has been subtracted by $\theta_{comp}{}'$ before phase error estimation, the estimated phase error can be described as below where the $\theta_{r,0}$ and $\theta_{r,1}$ are the mean and the linear phase error of pilots. The following equations explain the

33

behavior of Figure 2.23.

$$\theta_{comp}' = \begin{cases} \theta_0' & , \text{for } N_{sym} \leq N_{comp} \\ \theta_0' + \theta_1' & , \text{for } N_{sym} > N_{comp} \end{cases} \tag{2.25}$$

$$\theta_0 = \theta_{r,0} - \theta_0' \tag{2.26}$$

$$\theta_1 = \begin{cases} \theta_{r,1} & , \text{for } N_{sym} \leq N_{comp} \\ \theta_{r,1} - \theta_1' & , \text{for } N_{sym} > N_{comp} \end{cases} \tag{2.27}$$

$$\begin{aligned} \theta_{0,comp} &= W_0\theta_0 + \theta_0' = W_0\theta_{r,0} + (1-W_0)\theta_0' \\ &= W_0\theta_{r,0,N_{sym}} + W_0 \sum_{m=1}^{N_{sym}-1} (1-W_0)^{N_{sym}-m} \theta_{r,0,m} \end{aligned} \tag{2.28}$$

$$\begin{aligned} \theta_{1,comp} &= \begin{cases} W_1\theta_1 + (1-W_1)\theta_1' & , \text{for } N_{sym} \leq N_{comp} \\ W_1\theta_1 + \theta_1' & , \text{for } N_{sym} > N_{comp} \end{cases} \\ &= W_1\theta_{r,1} + (1-W_1)\theta_1' \\ &= W_1\theta_{r,1,N_{sym}} + W_1 \sum_{m=1}^{N_{sym}-1} (1-W_1)^{N_{sym}-m} \theta_{r,1,m} \end{aligned} \tag{2.29}$$

At first, the recently received pilots have to be compensated with the phase error in previous estimation. The estimated phase error outputted from the least squares estimator has to be jointed into the weighting function to estimate the latest phase error. The latest phase can be used to compensate the other carriers' data. It is also input into the storage for the estimation of the next symbol. Equation (2.28) and equation (2.29) are the estimated mean phase error and the linear phase error. They are the compensated angle, too.

We also use some mechanisms to avoid making a wrong estimation. The first one is to add an evaluation time. At the start of a transmission, we have to observe several symbols to get a more correct tendency. The symbol number is N_{comp}. From equation (2.25) to equation (2.29) and Figure 2.23, we know that if the symbol index is smaller

than N_{comp}, the SCO compensation is stopped. In the evaluation time, the estimation is continuous and the weighting functions are different. The second method is to judge if the estimation result is reasonable. If these slops between different pilots' phase have the same trend, the estimation result will be accepted. In a low SNR environment, the noise will make a violent change on each pilot. Accepting the estimation hastily may cause an excessive response and need a long time to mitigate the memory effect of wrong estimation in the feedback loop. In chapter 5, the mechanism will be implemented upon an application.

Chapter 3

THE PROPOSED DESIGN

In this section, adaptive channel equalization and phase noise compensation scheme will be proposed. The target OFDM system is the packet-based and burst synchronization scheme. In a real system, several synchronization issues must be taken care including frame detection (FD), multipath cancellation, and other channel effects. In our design, we will considerate not only our function blocks but also the whole system.

The total compensation scheme contains two partitions. One is the adaptive channel equalization for singular channel condition. The other is phase noise acquisition and compensation to make up the overall system require. This chapter is the distinguishing feature in the thesis.

3.1 Singular Channel Problem

Although there have been already many frequency domain deconvolution techniques [20], they are still not suitable in our situation because multipath may be composed of severe selective fading and unstable poles instead of convergent filtering. Besides, these existing frequency domain methods which produce aliasing CFR require more hardware cost. Another issue is the problem of traditional one-tap equalization, which noise would be enhanced largely on very deep channel frequency response. This effect shown in Figure 3.1 makes the performance unpredictable. As a result, we are going to propose a novel adaptive frequency domain approach to overcome the

36

significant issue.
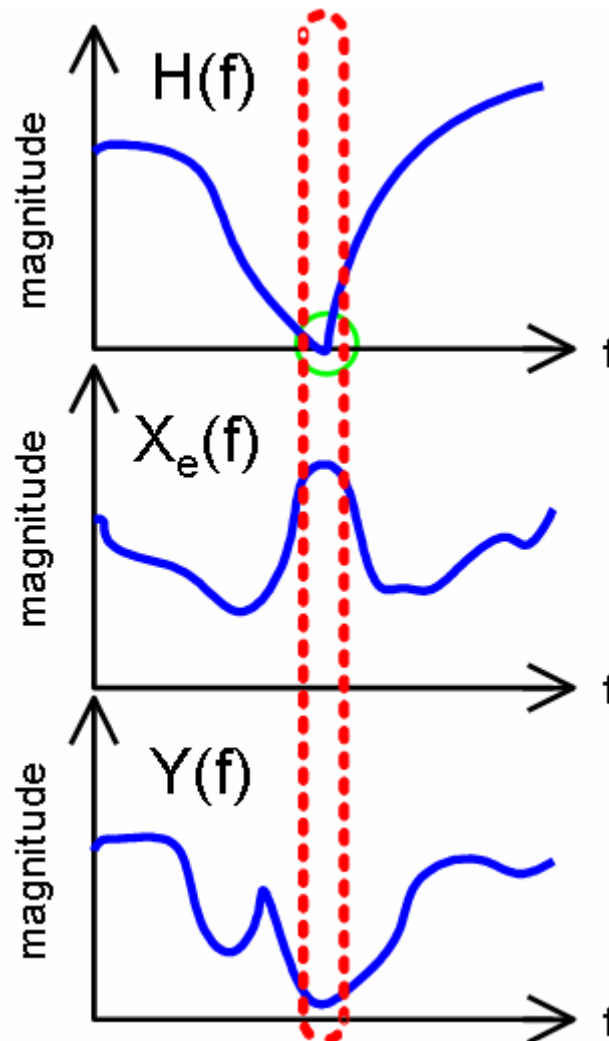
Figure 3.1 Noise would be enhanced largely on very deep CFR.

3.2 Adaptive Channel Estimation

In OFDM systems, instead of TDE, FDE is used to remove the influence of multipath fading channel, which requires less computation. In an ERP-OFDM of 802.11g packet, the received long preamble, $Y_L(k)$, is used for CFR estimation, where the estimated CFR, $H_E(k)$, can be derived as

$$H_E(k) = \frac{Y_L(k)}{X_L(k)} \tag{3.1}$$

$X_L(k)$ indicates the known long preamble data. Owing to the AWGN in long preamble, equalization is not perfect and causes data drift. Time domain CFO and SCO acquisition are also influenced by AWGN. These residual offsets after time domain compensation still causes received data incorrect. To remove the imperfect factors left in frequency domain, a joint scheme is proposed to remove the equalization error, residual CFO and SCO simultaneously with channel equalization.

The adaptive CE using smooth filter (SF) and decision-directed channel error tracking (DDCET) is proposed for high performance and low design complexity. SF has been applied to provide high performance and low complexity for CE [7], but the noise floor problem degrades performance in high SNR conditions. Combining SF and DDCET can enhance the total performance. The block diagram of the proposed scheme is given in Figure 3.2.
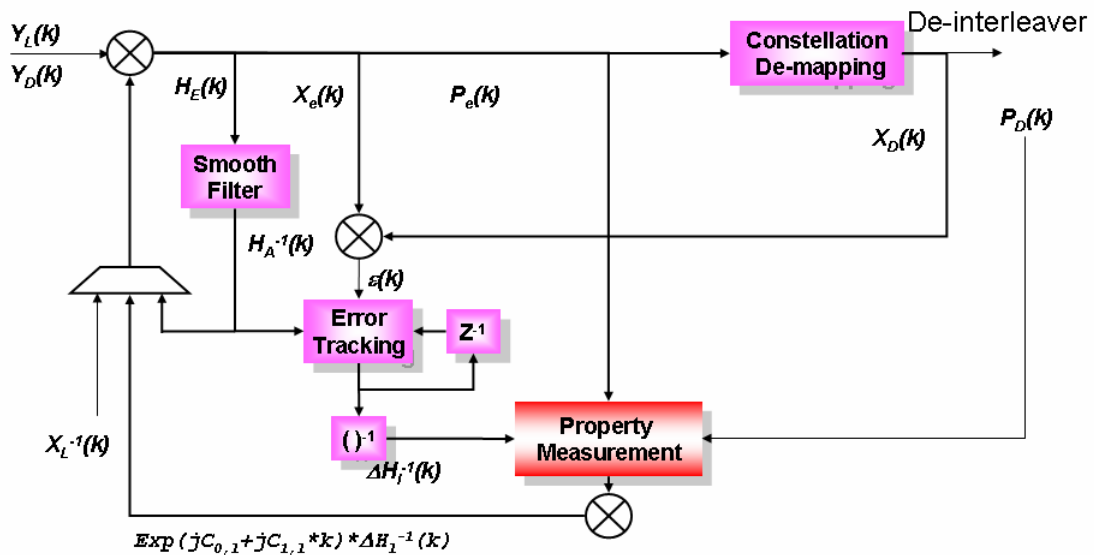
Figure 3.2 Block diagram of the adaptive EQ with PR.

38

For channel estimation, the inverse of known preamble, $X_L^{-1}(k)$, is selected to multiply with the received preamble, $Y_L(k)$. Smooth filter is then used to reduce the AWGN of estimated CFR, $H_E(k)$. For basic channel equalization, received data, $X_e(k)$, is multiplied with the estimated CFR, $H_A(k)$. However, in order to remove the CE error, residual CFO and SCO, an error estimator is applied to trace the compensation value. The estimator includes a feedback decision-directed channel estimation (DDCE), which is used to trace the equalization error by using the de-mapping information of the received data; and a weighted phase recovery, which is used to trace the residual CFO and SCO by using the phase information between the received pilots, $P_e(k)$, and the known pilots, $P_D(k)$. A joint compensation value is then feedback to the equalization operation; remove imperfect factors of the next OFDM symbol altogether with the original equalization multiplier. That is, CE error, residual CFO, and SCO are compensated with equalization simultaneously. Detail algorithms are discussed below.
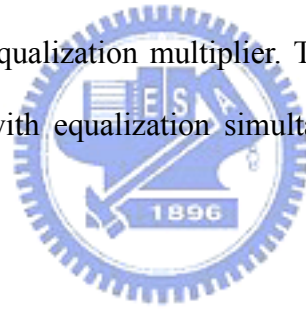
3.2.1 Fixed-coefficient Smooth Filter

The proposed smoothing filter is a finite impulse response (FIR) filter with exponential-decay power. The smoothing function is described as

$$S(k) = \frac{\sum_{\ell=-W_S}^{W_S} \delta(k-\ell)e^{-|\ell|R_S}}{\sum_{\ell=-W_S}^{W_S} e^{-|\ell|R_S}} \tag{3.2}$$

After estimation by dividing long preamble, the estimated CFR, $H_E(k)$, will be convoluted by the proposed smoothing filter. The convolution equation is listed as

$$H_S(k) = \sum_{\ell=-W_S}^{W_S} H_E(k-\ell)S(\ell) \qquad (3.3)$$

After the filter, each subcarrier of CFR will be weighted summation of itself and nearby subcarriers within $2W_S+1$ bandwidth. And the weighting function is equal to filter coefficient $\ell \cdot R_S$. Since additive noise is zero-mean, the weighted summation will decrease the noise power. Assume that $H(k)$ is the true CFR; $W_L(k)$ is the frequency-domain additive noise in long preamble; and $\varepsilon_{HS}(k)$ is the noise of smoothing filter. The smoothed CFR, $H_S(k)$, can be described as

$$H_S(k) = \frac{Y_L(k)}{X_L(k)} + \varepsilon_{HS} = \frac{X_L(k)H(k)+W_L(k)}{X_L(k)} + \varepsilon_{HS} = H(k) + \frac{W_L(k)}{X_L(k)} + \varepsilon_{HS} \qquad (3.4)$$

In low SNR regions, smoothing noise, $\varepsilon_{HS}(k)$, can be deal with the additive noise, $W_L(k)/X_L(k)$, efficiently. In high SNR regions, however, the additive noise power will be neglected and the smoothing noise will dominate the estimation error and degrade the estimation performance. Thus we can find

$$\begin{cases} \left| \varepsilon_{HS}(k) + \dfrac{W_L(k)}{X_L(k)} \right| \approx \left| \varepsilon_{HS}(k) \right|, \ if \ \left| \varepsilon_{HS}(k) \right| \gg \left| \dfrac{W_L(k)}{X_L(k)} \right| \\[4mm] \left| \varepsilon_{HS}(k) + \dfrac{W_L(k)}{X_L(k)} \right| < \left| \dfrac{W_L(k)}{X_L(k)} \right|, \ otherwise \end{cases} \qquad (3.5)$$

From equation (3.5), we find the estimation error will saturate to smoothing noise in high SNR regions. Thus the smoothing filter is suitable for low SNR regions. And in high SNR regions, the proposed adaptive channel manager will detect the error saturation and select estimated CFR, $H_E(k)$, instead of smoothed CFR, $H_S(k)$, for

equalization.

3.2.2 Adaptive Channel Manager

In high SNR regions, since the smoothing noise degrades the estimation performance, adaptive channel manager will select estimated CFR as the adapted CFR, $H_A(k)$. It detects saturation of estimation error by receiving the information, L_{SNR}, about SNR from AGC. We can get the SNR criterion, L_0, with the saturation noise from the simulation. Dependent on L_0, the adapted CFR will be selected as

$$\begin{cases} H_A(k) = H_S(k), \; if \; L_{SNR} \geq L_0 \\ H_A(k) = H_E(k), \; if \; L_{SNR} < L_0 \end{cases} \tag{3.6}$$

From the algorithm, adaptive channel manager use the SNR criterion for selection of adapted CFR. The adapted CFR can be described as

$$H_A(k) = H(k) + \varepsilon_{HA}(k), \; where \; \varepsilon_{HA}(k) = \begin{cases} \dfrac{W_L(k)}{X_L(k)} + \varepsilon_{HS}(k), \; if \; L_{SNR} \geq L_0 \\ \dfrac{W_L(k)}{X_L(k)} \qquad , \; if \; L_{SNR} < L_0 \end{cases} \tag{3.7}$$

By means of adaptive channel manager, channel estimation error will never saturate in high SNR regions and the performance is enhanced. After receiving preamble, adapted CFR will be inversed and stored in inversed CFR buffer. The residual estimation error, $\varepsilon_{HA}(k)$, will be traced and removed in decision-directed tracking loop described in the following section.

3.2.3 Feedback Decision-directed Channel Error Tracking

Feedback DDCET is applied for high performance and low complexity. Computation-save control (CSC) is applied in DDCET to reduce redundant tracking. Channel error tracking can be turned off after several OFDM symbols cause the tracking error is converged to a very small value. The feedback DDCET estimates the CFR error by the de-mapping result of data subcarriers. In data transmission, the equalized data subcarriers with CFR, $H_A(k)$, can be shown as

$$X_e(k) = \frac{Y_D(k)}{H_A(k)} = \frac{X_D(k) \cdot H(k) + W_i(k)}{H_A(k)} = \frac{X_D(k) \cdot [H_A(k) - \Delta H(k)] + W_i(k)}{H_A(k)} \quad (3.8)$$

where $W_i(k)$ indicates the frequency-domain additive noise in data subcarriers. The estimated CFR error, $\Delta H(k)$, causes the de-mapping error vector between the equalized carrier, $X_e(k)$, and the predicted de-mapping signal, $X_D(k)$. This error vector can be derived as

$$\varepsilon(k) = X_e(k) - X_D(k) = \left(\frac{-X_D(k) \cdot \Delta H(k)}{H_A(k)} + \frac{W_i(k)}{H_A(k)} \right) \quad (3.9)$$

For CFR error estimation, this DDCET uses the mean of normalized constellation error vectors to eliminate the zero-mean additive noise, $W_i(k)$. The mean of the normalized constellation error vectors during *l* OFDM symbols is listed as

$$m_\varepsilon(k) = \frac{1}{l}\sum_{N=1}^{l}\varepsilon_N(k)\cdot X_{D,N}(k)^{-1} = \frac{-\Delta H_N(k)}{H_A(k)} + \frac{\sum_{N=1}^{l}W_{i,N}(k)}{H_A(k)\cdot X_{D,N}(k)}$$
$$\approx \frac{-\Delta H_N(k)}{H_A(k)}\ for\ l\to\infty\ \left(\because m_{W_i}=0\right) \tag{3.10}$$

Unlike the feedforward compensation method, we use feedback scheme to get better performance and less compensation complexity. In the feedback loop, the CFR, $H_A(k)$ is adjusted by the running average of estimated CFR error, $\Delta H(k)$.

$$\Delta H_l(k) \approx -H_A(k)\cdot m_\varepsilon(k) \tag{3.11}$$

After that, we compare the equalized pilots with the known one and compute the mean-square error as the error function. Then we judge if this corrected CFR is suitable. If the MSE of the equalized pilots, MSE_{comp}, is greater than the MSE of the pilots before compensated, MSE_{ori}, we discard this CFR. Otherwise, the old CFR will be replaced by the suitable one. The algorithm of this feedback loop is

$$MSE_{ori} = \frac{1}{M}\sum_{k=1}^{M}\left|P_e(k)-P_D(k)\right|^2 \tag{3.12}$$

$$MSE_{comp} = \frac{1}{M}\sum_{k=1}^{M}\left|P_e(k)\cdot[H_A(k)-\mu\Delta H_{l-1}(k)]^{-1}-P_D(k)\right|^2 \tag{3.13}$$

$$H_{A,l}(k) \approx \begin{cases} H_A(k)-\mu\cdot\Delta H_{l-1}(k), & if\ MSE_{comp} > MSE_{ori} \\ H_A(k) & ,\ if\ MSE_{comp} \le MSE_{ori} \end{cases} \tag{3.14}$$

where M is the number of pilots and μ is the step size of the adaptive tracking loop. Under the feedback tracking algorithm which adjusts the CFR directly instead of compensating the data subcarriers only, we can get more accurate data subcarriers to

make more precise estimations of CFR error, residual CFO and SCO, hence a better system performance.

Table 3.1 Summary of the proposed equalizer.

Initialization: $H_E(k) = \dfrac{Y_L(k)}{X_L(k)}$

For each new OFDM symbol arriving at the equalizer

Smoothing: $H_A(k) = H_E(k) \otimes S(k)$

De-mapping error vector: $\varepsilon(k) = X_e(k) - X_D(k)$

Mean of normalized constellation error vectors: $m_\varepsilon(k) \approx \dfrac{-\Delta H_N(k)}{H_A(k)}$

Residual estimation error: $\Delta H_l(k) \approx -H_A(k) \cdot m_\varepsilon(k)$

Property Measurement:

$$\sum_{k=1}^{M} \left| P_e(k) \cdot [H_A(k) - \mu \Delta H_{l-1}(k)]^{-1} - P_D(k) \right|^2 - \sum_{k=1}^{M} \left| P_e(k) - P_D(k) \right|^2$$

Adaptation: $H_{A,l}(k) = H_A(k) - \mu \cdot \Delta H_{l-1}(k)$

End

3.3 Phase Noise Detection and Compensation

When phase noise occurs, the accuracy of CFO estimator will descend following the performance degradation. The phase deviation in frequency domain is not linear anymore. One reason is that the increased remaining frequency offset makes the ICI playing an important role in the effect of CFO. Besides, the additional phase noise, $B\sin\Delta\omega t$, causes extra phase shift in each OFDM symbol. That means the phase

difference between two repeat OFDM symbols is not the same. In frequency domain, phase gain between two adjacent OFDM symbols can be described as

$$y_n = x_n e^{-j2\pi n T_s [\Delta f + \phi(t)]} \tag{3.15}$$

$$Y_{l,k} = e^{-j2\pi l N_G T_S (\Delta f + \phi(t))} X_{l,k} \text{ (ignore ICI)} \tag{3.16}$$

$$Y_{l-1,k} = e^{-j2\pi(l-1)N_G T_S (\Delta f + \phi(t-1))} X_{l-1,k} \tag{3.17}$$

$$\sum_{i=1}^{l} C_{0,i} = \theta_l = -2\pi l N_G T_S (\Delta f + \phi(t)) \tag{3.18}$$

$$
\begin{aligned}
C_{0,l} &= \theta_l - \theta_{l-1} \\
&= -2\pi l N_G T_S (\Delta f + \phi(t)) + 2\pi(l-1)N_G T_S (\Delta f + \phi(t - N_G T_S)) \\
&= -2\pi N_G T_S \Delta f - 2\pi N_G T_S \phi(t - N_G T_S) \\
&\quad -2\pi l N_G T_S \phi(t) + 2\pi l N_G T_S \phi(t - N_G T_S) \\
&= -2\pi N_G T_S \Delta f - 2\pi N_G T_S [l\phi(t) - (l-1)\phi(t - N_G T_S)] \\
&= -2\pi N_G T_S \Delta f - 2\pi N_G T_S \{lB \sin[\Delta\omega(lN_G + k)T_S] \\
&\quad -(l-1)B \sin[\Delta\omega((l-1)N_G + k)T_S]\}
\end{aligned}
\tag{3.19}
$$

Obviously, we can not calculate the exact remaining frequency offset from equation (3.19) because the phase shift increases in some OFDM symbols and decreases in other OFDM symbols.

Hence, we need a new mechanism against the degradation due to phase noise. The proposed phase noise detection algorithm can be separate into two steps. Step one is phase noise acquisition. In this stage, we record the tendency of remaining CFO which we can get from PR. A search window storing 2c results is used for searching peak of fluctuating wave caused by phase noise. The minimum error tolerance for peak decision is e/c. Once detecting peak, keep the corresponding OFDM symbol number, *l*. After the second peak obtained, we can estimated loop time constant, Δω, with equation (3.20). Figure 3.3 shows the search window with error tolerance and

phase deviation arise from phase noise.

$$\Delta\omega = \frac{1}{T} = \frac{1}{(l'-l)N_G T_S}$$ (3.20)
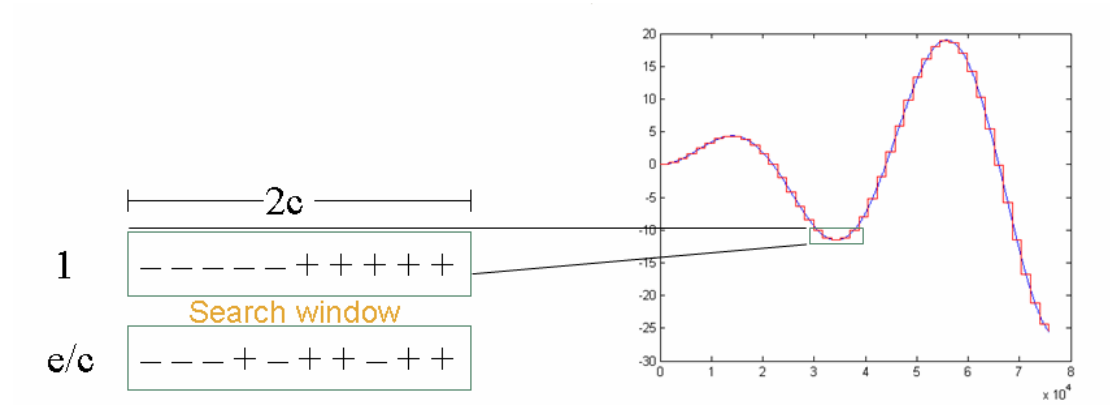

Figure 3.3 Search window of the proposed phase noise detection.

The other parameter, loop bandwidth, can be estimated by relationship between loop time constant and phase difference of peaks.

$$B = \frac{C_{0,l} - C_{0,l-1}}{-2\pi N_G T_S}$$
$$\times \{l\sin(\Delta\omega(lN_G + k)T_S) - 2(l-1)\sin[\Delta\omega((l-1)N_G + k)T_S]$$ (3.21)
$$+ (l-2)\sin[\Delta\omega((l-2)N_G + k)T_S]\}^{-1}$$

After phase noise parameters are calculated, the correct data can be obtained from the time domain before FFT. The compensation architecture starts to generate *sin* wave joint with estimated CFO to correct the phase of the received data. The block diagram is shown in Figure 3.4.
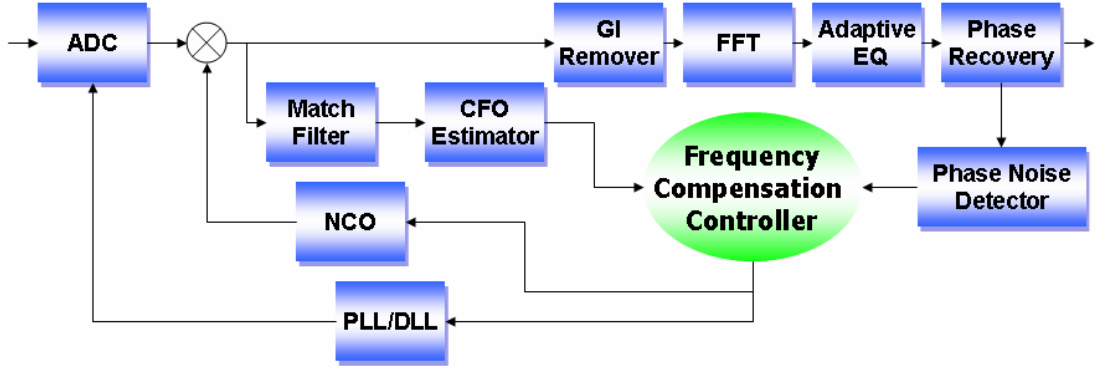
Figure 3.4 Block diagram of the proposed design.

Although the compensation engine started, the high frequency noise makes the phase of the received data drifting. Therefore, step two – phase noise tracking is turn on. From section 2.2.3.2, we know that the remaining CFO will be limited in 1 ppm. If the detected value is more than that after phase noise compensation, we can assert that the acquisition is not accurate enough. Assume the loop time constant has more credit (error rate > 90%), we adjust loop bandwidth, B, in binary search to approach the real value. The initial margin can be obtained by equation (3.22).

$$
\begin{aligned}
\Delta B &= B - \hat{B} \\
&= \frac{C_{0,l} - C_{0,l-1}}{-2\pi N_G T_S} \\
&\quad / \{l\sin(\Delta\omega(lN_G + k)T_S) - 2(l-1)\sin[\Delta\omega((l-1)N_G + k)T_S] \\
&\quad + (l-2)\sin[\Delta\omega((l-2)N_G + k)T_S]\}
\end{aligned}
\tag{3.22}
$$

$$
B = \hat{B} + \Delta B
\tag{3.23}
$$

If the current remaining CFO, C_0, is larger than last one, $C_{0,old}$, increase B. On the other hand, decrease B with the estimated bandwidth error, ΔB. When the fixed bandwidth is out of range (> 50 ppm), we discard the result and return to acquisition stage. With the help of binary search, the loop bandwidth will finally converge and

loop time constant will be refined at the same time. The estimated parameters will be store and update for the next packet, so the compensation mechanism can directly modify the received signal after first packet. Correctly speaking, not only the AFC but also other synchronization blocks can avoid suffering from distortion of phase noise. The compensation step of each field in OFDM packet is shown in Figure 3.5.
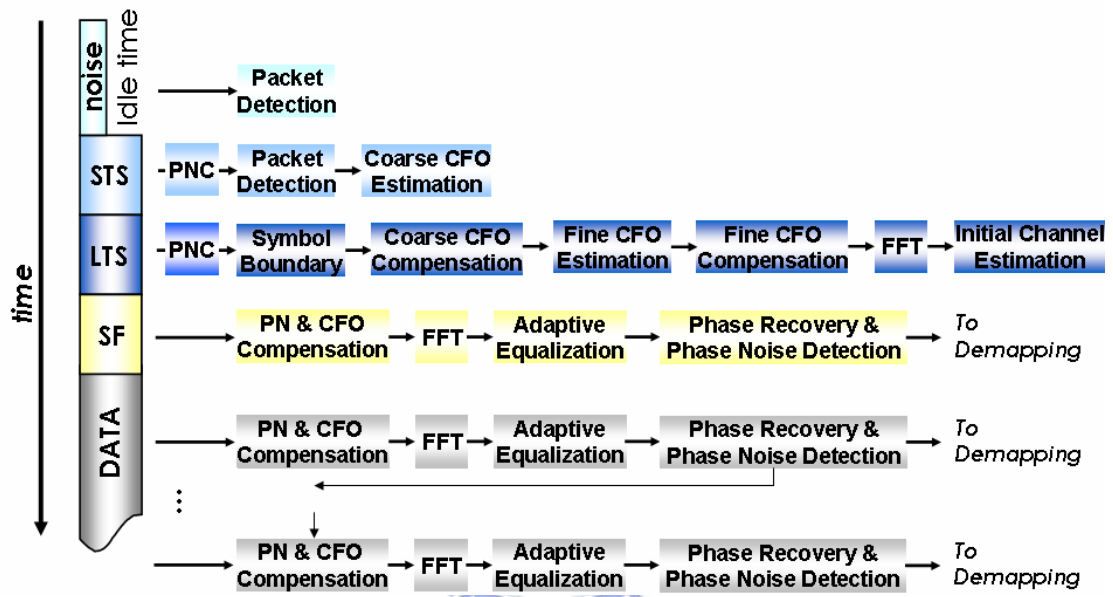

Figure 3.5 Compensation engine of the proposed design.

Chapter 4
PERFORMANCE ANALYSIS

To satisfied system requirement, system PER is simulated under the highest data rate
of IEEE 802.11g, which is the 54 Mbps mode with 64-QAM modulation and 3/4 FEC
coding rate [3]. In simulations with multipath channel, IEEE Rayleigh-fading channel
is used with different RMS delay spread and 13 independent taps. We also assume a
fading channel varying from packet to packet; i.e., it is static within each packet, and
the required performance is measured at a PER of 10%. In below performance
analysis, system PER of the proposed adaptive equalization and phase noise detection
will be discussed and compared with the conventional approaches.

4.1 Adaptive Channel Equalization

Table 4.1 SNR degradation under different modulation with singular channel.

Modulation	BPSK	QPSK	16-QAM	64-QAM
SNR degrade (dB)	3	5	7	10

Comparison of the conventional feedforward equalization and the proposed adaptive
equalization is shown is Figure 4.1. From this figure, we know that the conventional
method needs additional compensation hardware. On the other hand, the proposed
algorithm adjusts the channel frequency response instead of fix compensation. The
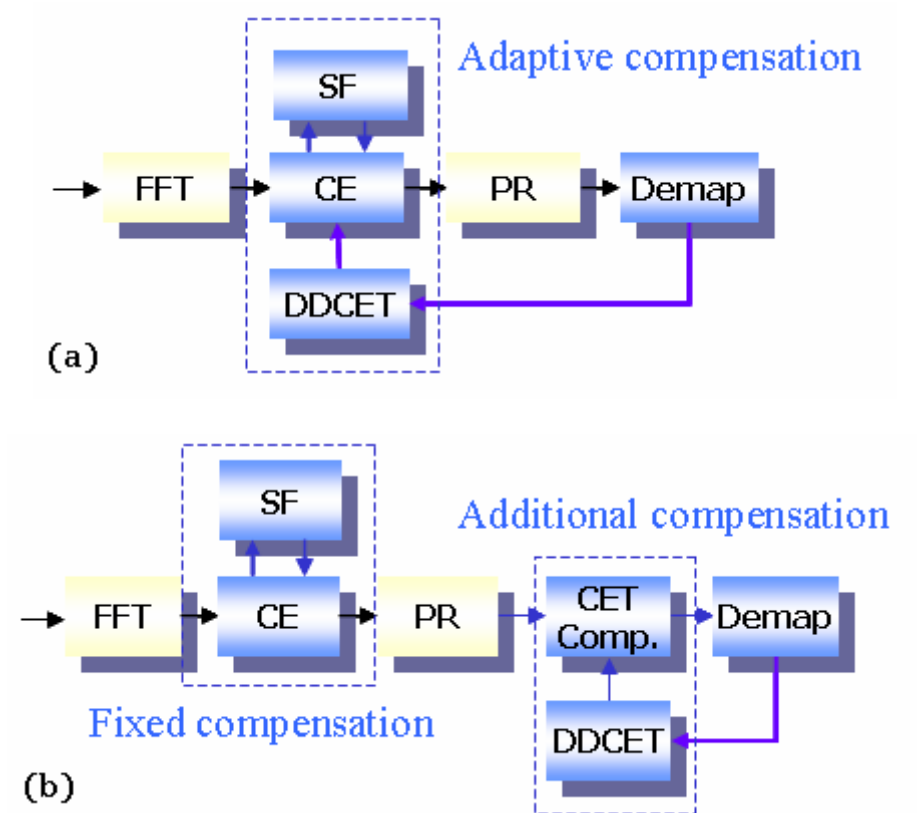approach not only saves cost but also maintains accuracy.

Figure 4.1 (a) The proposed feedback DDCET.

(b) Conventional feedforward DDCET

The brilliant performance of the proposed adaptive equalization in IEEE channel with RMS delay spread 25, 50 and 100 ns is shown in Figure 4.2 to 4.6. The singular channel which exists the very deep point in the CFR is 30% in the real world. And the other 70% channel we call them general or ordinary channel in the thesis. The singular channel which has low point in CFR degrades the performance larger as the modulation order increase. The result is shown in Table 4.1. From these simulation results, we can see that the proposed method has little help in the ordinary channel but obviously has a lot of improvement in the singular channel. And it even can resist the delay spread up to 100 ns while the traditional methods fail.
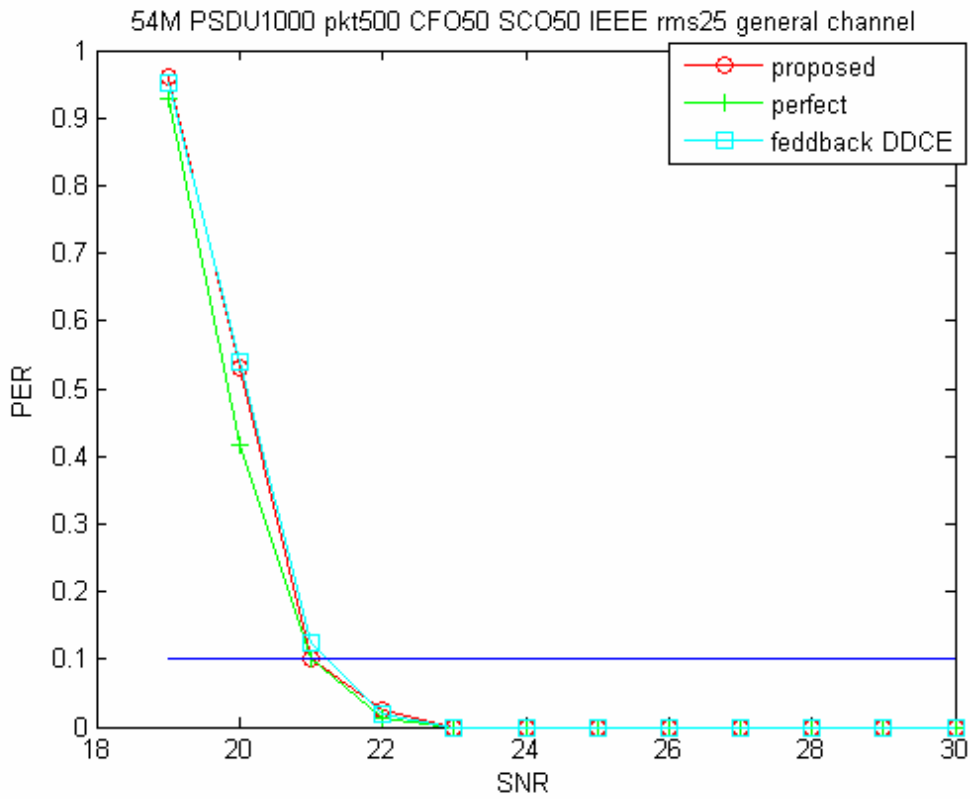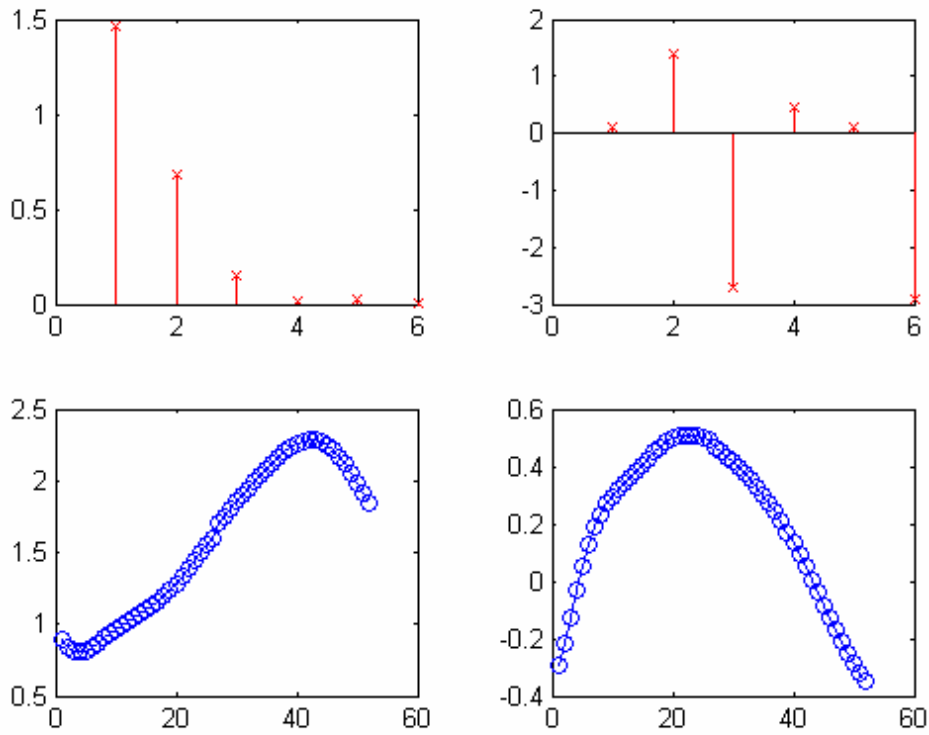
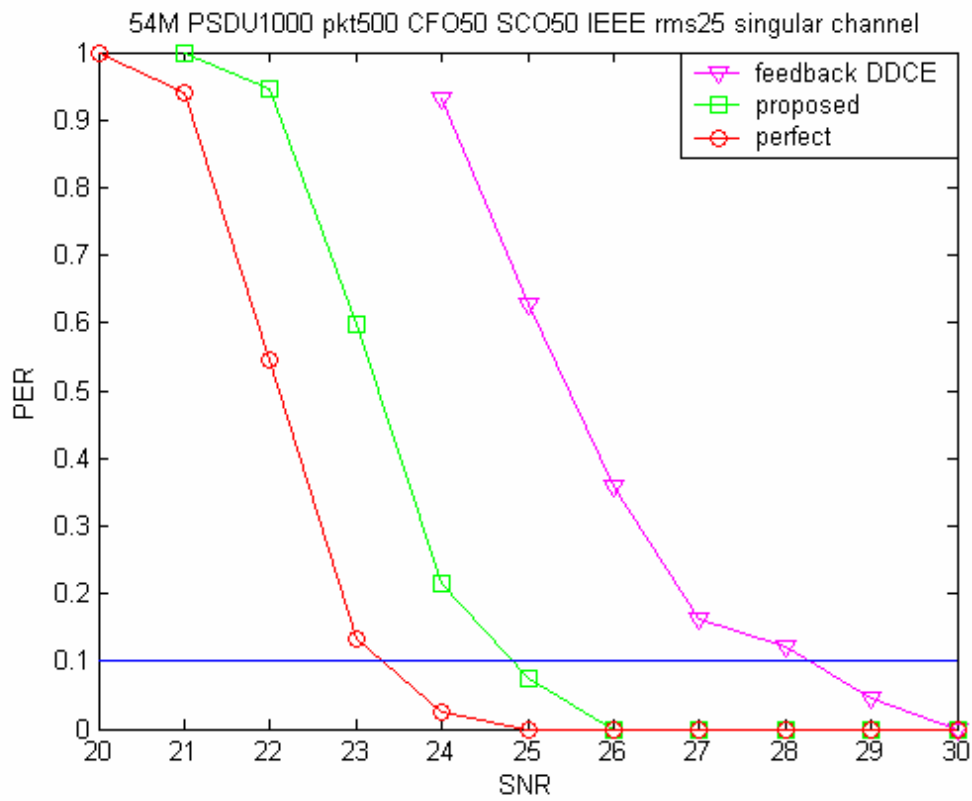**Figure 4.2** Performance of adaptive CE in IEEE rms 25 general channel.
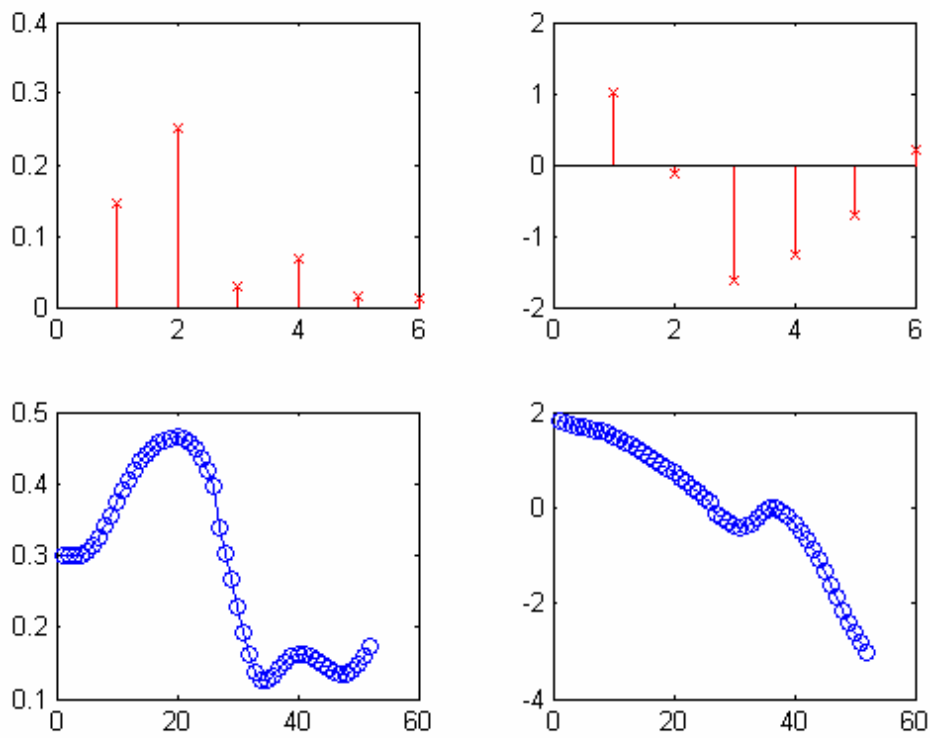
Figure 4.3 Performance of adaptive CE in IEEE rms 25 singular channel.
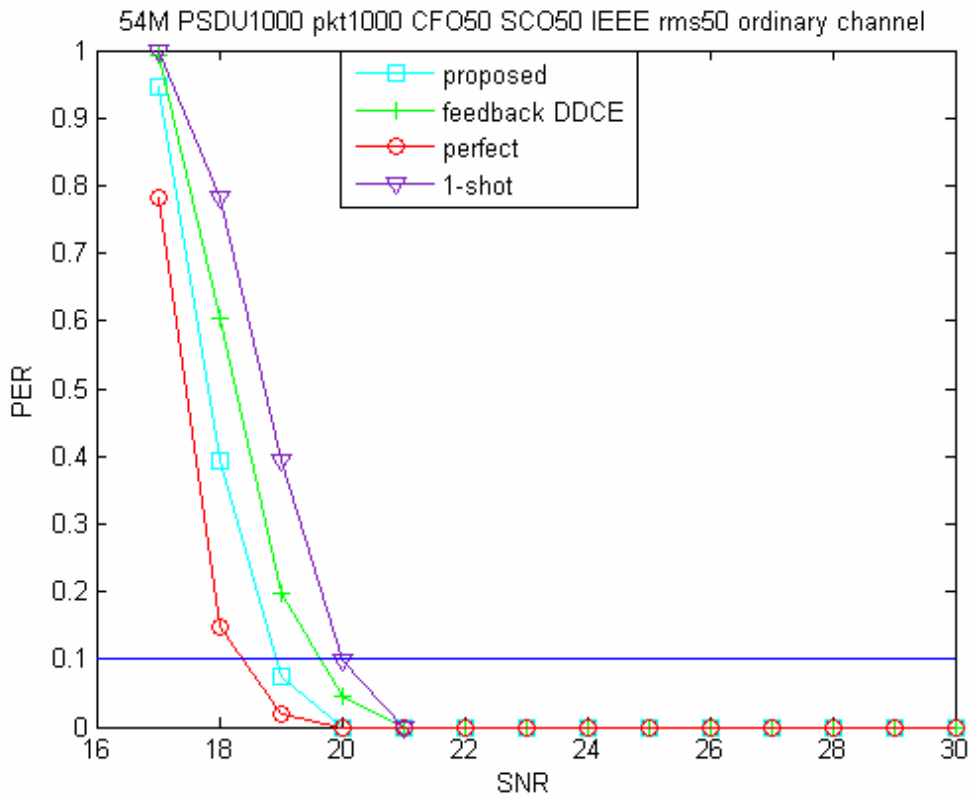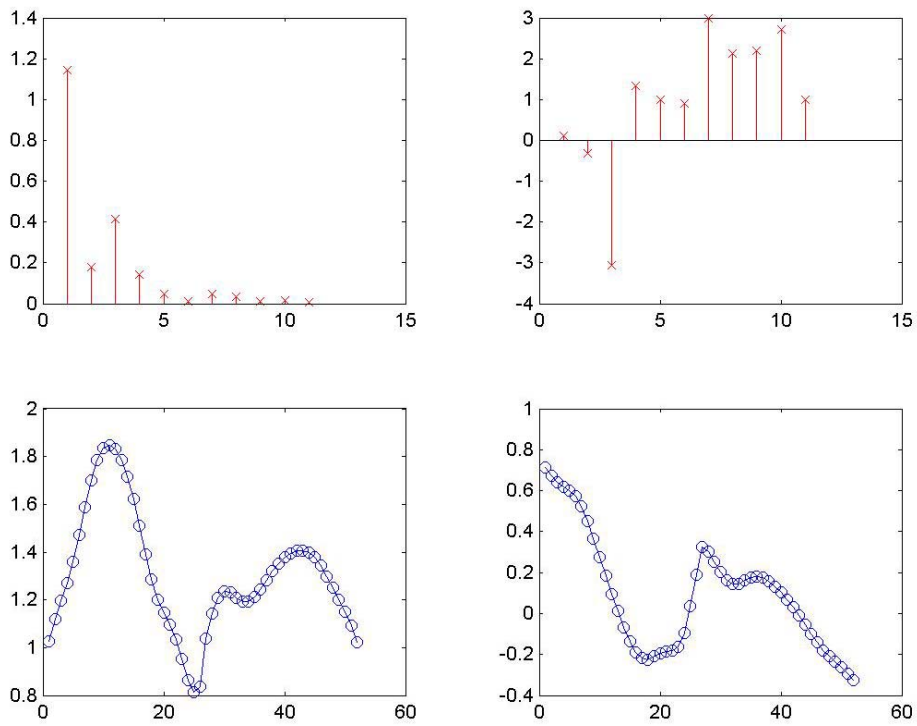
Figure 4.4 Performance of adaptive CE in IEEE rms 50 general channel.
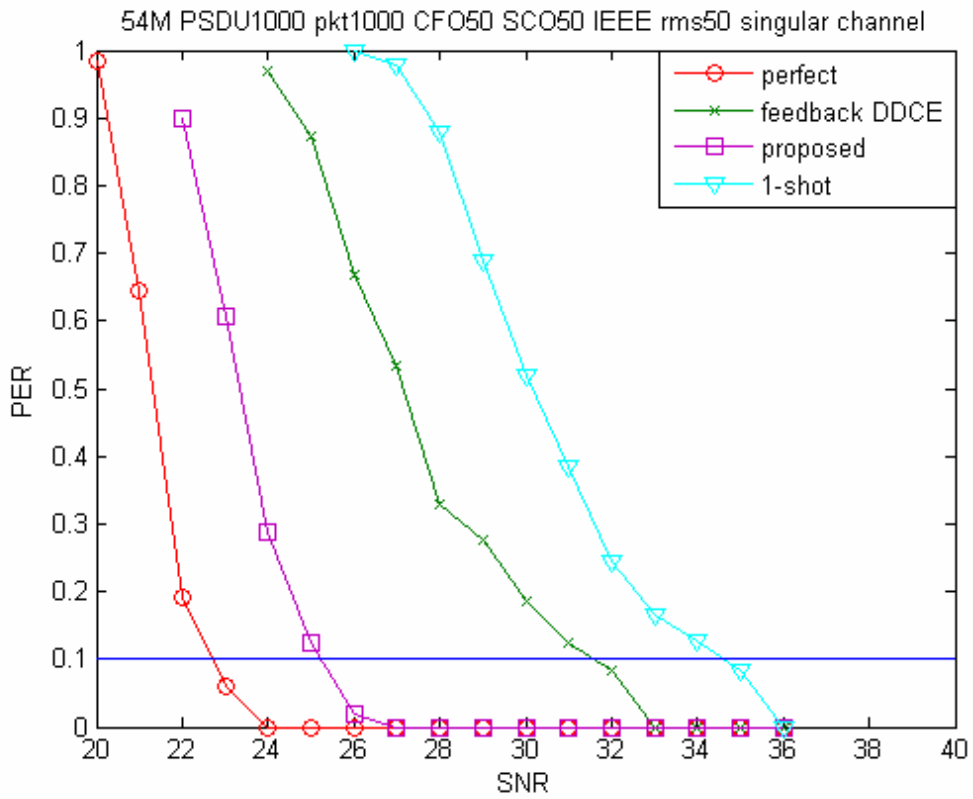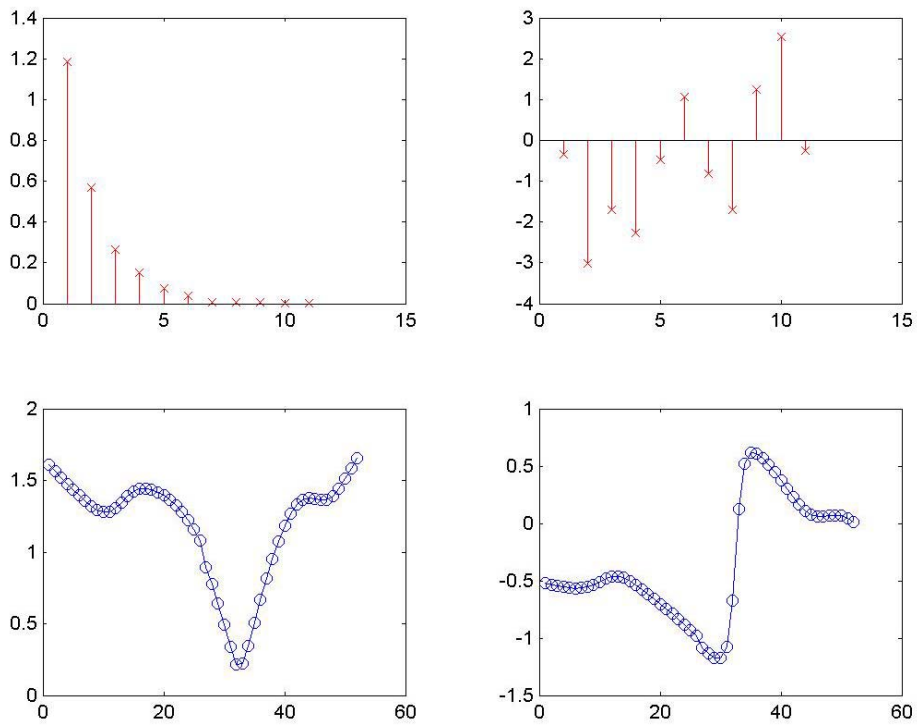
Figure 4.5 Performance of adaptive CE in IEEE rms 50 singular channel.
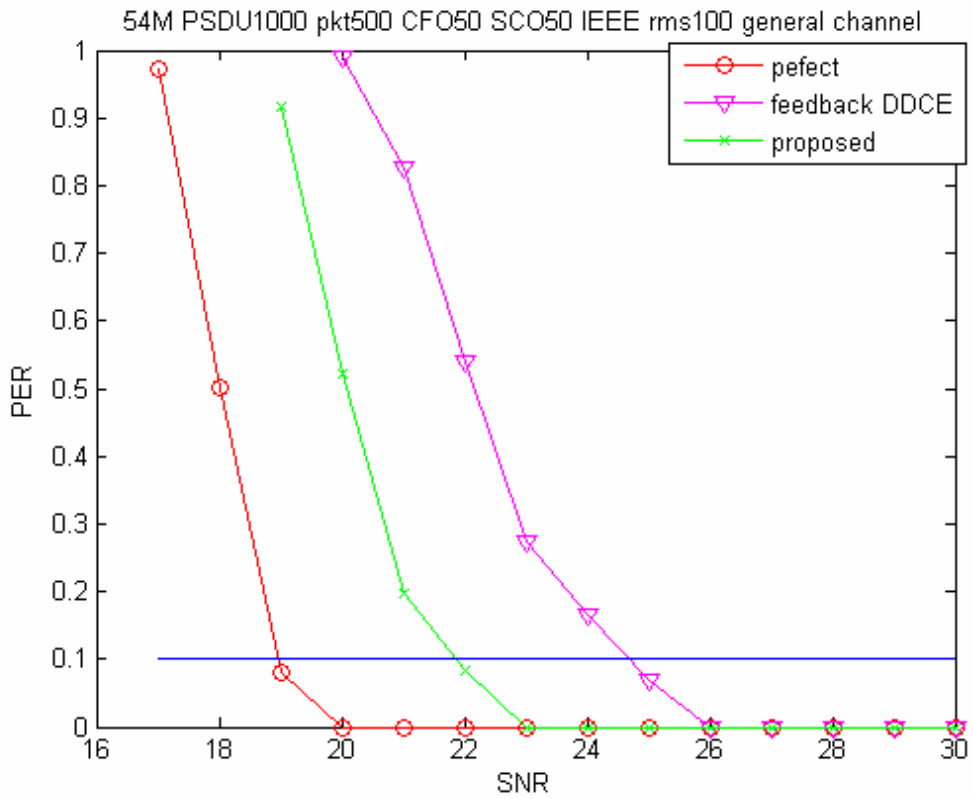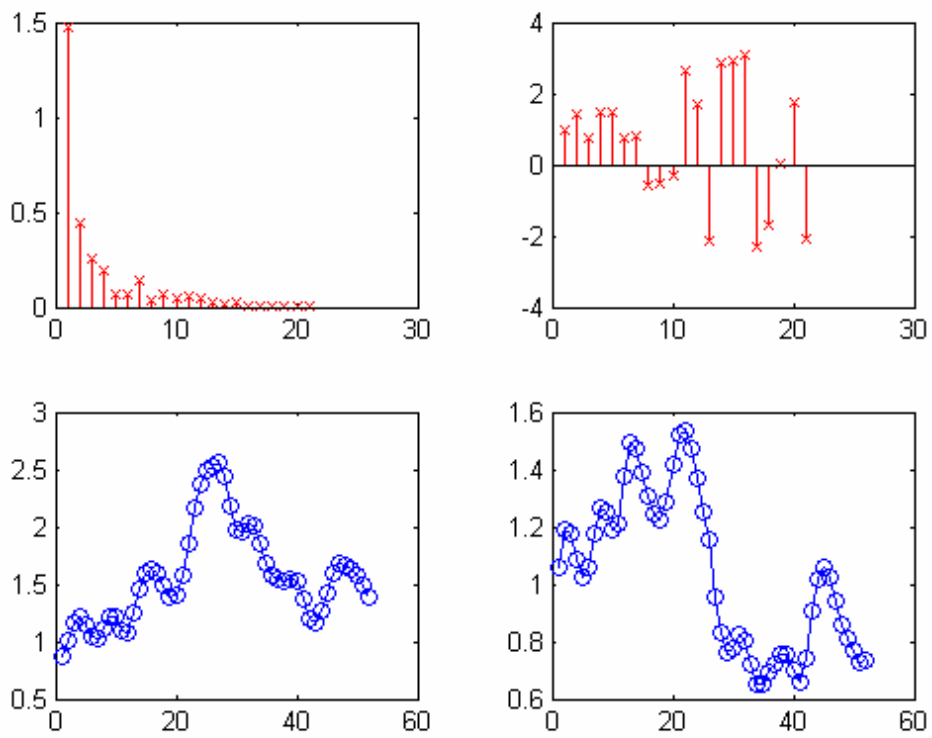
Figure 4.6 Performance of adaptive CE in IEEE rms 100 general channel.

Table 4.2 Comparison of the adaptive CE in different channel.

Channel Method	Ordinary (rms 50)	Singular (rms 50)
Perfect	18.3	22.7
This work	18.9	25.1
[7]	19.7	31.5
1-shot	20	34.8

In the proposed scheme, instead of estimating the compensation value of present OFDM symbol directly, the increasing rate estimation of compensation value is applied to predict the data drift of the present OFDM symbol using the information of the past symbols. In Figure 4.7, the estimated values of OFDM symbol index are shown. After about 20 OFDM symbols, tracking error is converged to a small value. Then the channel error tracking can be turned off.

Figure 4.7 Convergence of the proposed adaptive equalization.

Table 4.3 lists some adaptive equalization in the world. Most of the details are discussed in chapter 1. In short, we are the best of all.

Table 4.3 Comparison state-of-the-art adaptive equalization.

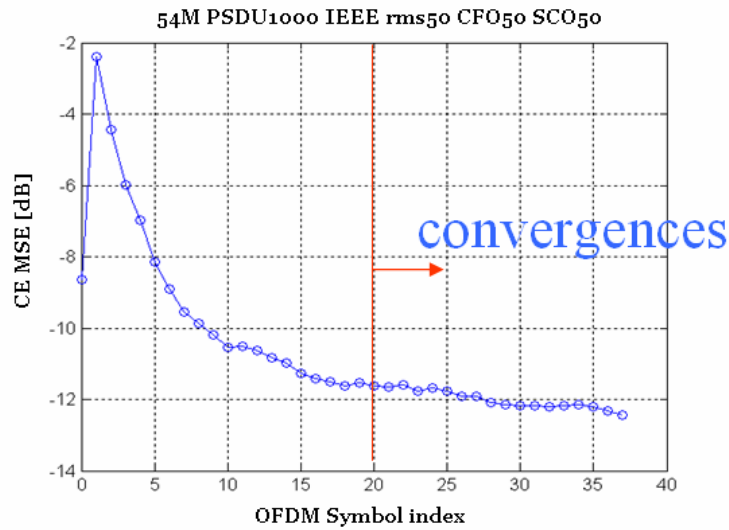|	ISCAS 2005 [12]	ICCS 2004 [13]	TCSET 2004 [14]	Globecom 2004 [15]	This work
Operating Domain	Time	Time	Time	Time	Frequency
Method	Weighted RLM	Reduced-rank modified LMS	MOE	LMS	Feedback DD
Property Utilization	Preamble	Pilot	GI	GI	Pilot
Modulation	N/A	QPSK	N/A	QPSK	64-QAM
Channel Condition	Random 12 taps	Typical Urban channel 7 taps	[-1.28-0.301j, -0.282+0.562j, 0.106+1.164j] 3 taps	[0.4, 0.85, 0.15, 0.3] 4 taps (delay is long and short)	IEEE rms 50 13 taps singular
Performance	Better than RLS & conventional RLM (MSE)	1dB degrades (perfect), 14dB better than 1-shot (SER 10^{-2})	3dB better than SOFDM, 10dB better than 1-shot (BER 10^{-2})	1dB degrades (perfect) (BER 10^{-2})	1dB degrades from perfect, 10dB better than 1-shot (PER 0.1)
Convergence Cycle	300 (sample)	400 (sample)	N/A	500 (symbol)	20 (symbol)
Characteristic	Capable of resist NBI	Does not require the channel statistics	Can handle channel delay > GI	Low complexity	has large improvement in singular channel
Overhead	Lack of BER and comparison with perfect	The smaller the rank the higher error level and the faster convergence speed	Redundant in low SNR, adaptive is unnecessary	Lack of fig. of MSE vs. OFDM #	Cost more hardware

4.2 Phase Noise Detection

Figure 4.8 shows the performance without the proposed phase noise detection and the profile of PER = 1. Figure 4.9 is the same condition except with our design. Compare these two figures, we can find that the phase noise tolerance is surprisingly improved. Note that the phase fluctuates dramatically over boundary ($\pm\pi$) when loop bandwidth is larger than 6 ppm, so performance degrades fast. Another thing deserve to be mentioned is that the detection algorithm doesn't work when loop time constant is less than 7 kHz when packet length equals to 1000 since it needs two peaks. Although the tolerance of our method is not enough large, the serious condition won't happens or no one can handle that situation. The so called cycle slip occurs when the carrier frequency changes from one edge to another edge quickly, e.g. from -50 ppm to 50 ppm with 100 kHz. In this situation, even we have good algorithm can still not save the performance loss.

Table 4.4 Comparison of the tolerance without and with phase noise detection.

Estimation property / Phase noise detector	Max loop bandwidth	Max loop time const.
without	7 ppm	1.1 kHz
with	11 ppm	25 kHz

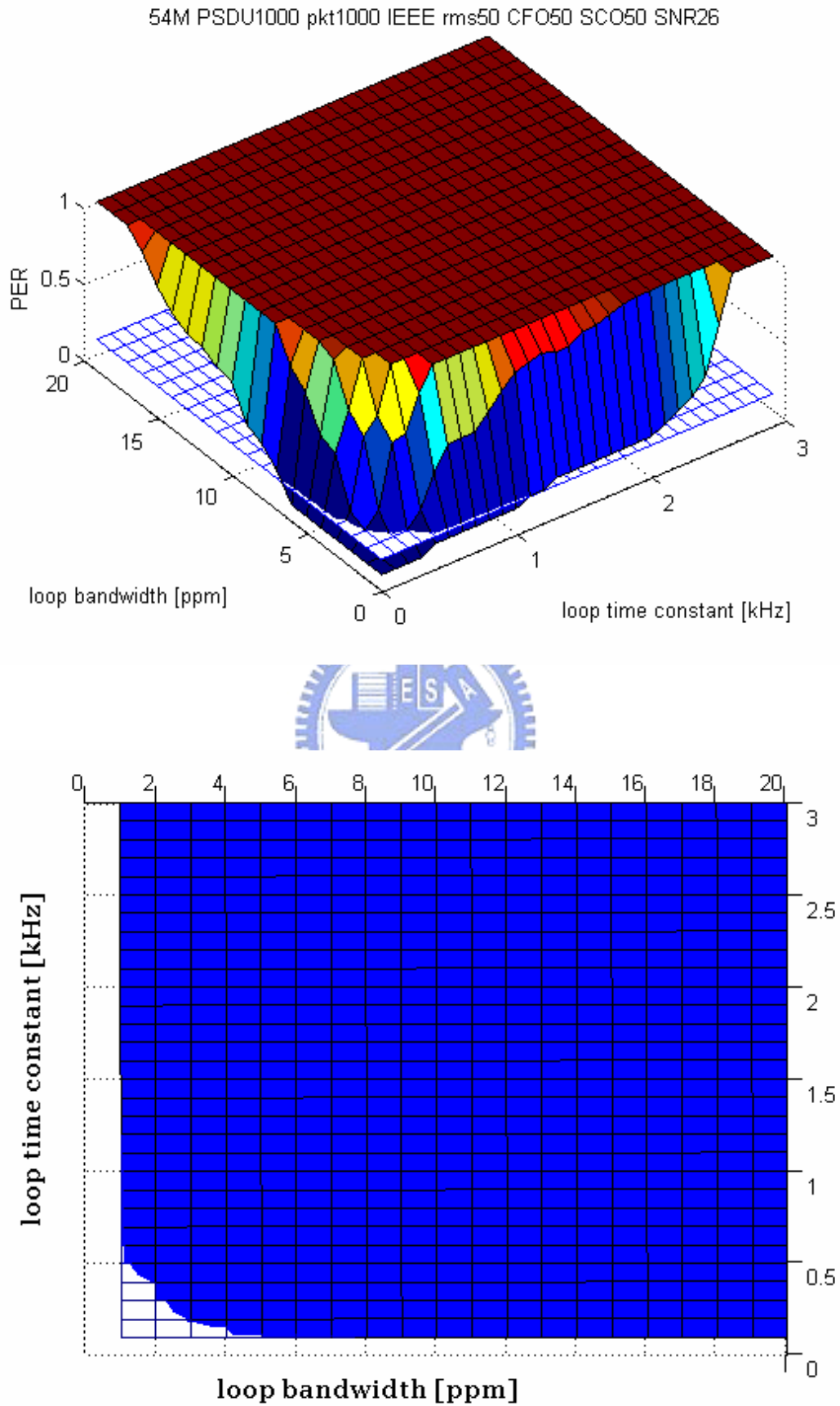54M PSDU1000 pkt1000 IEEE rms50 CFO50 SCO50 SNR26

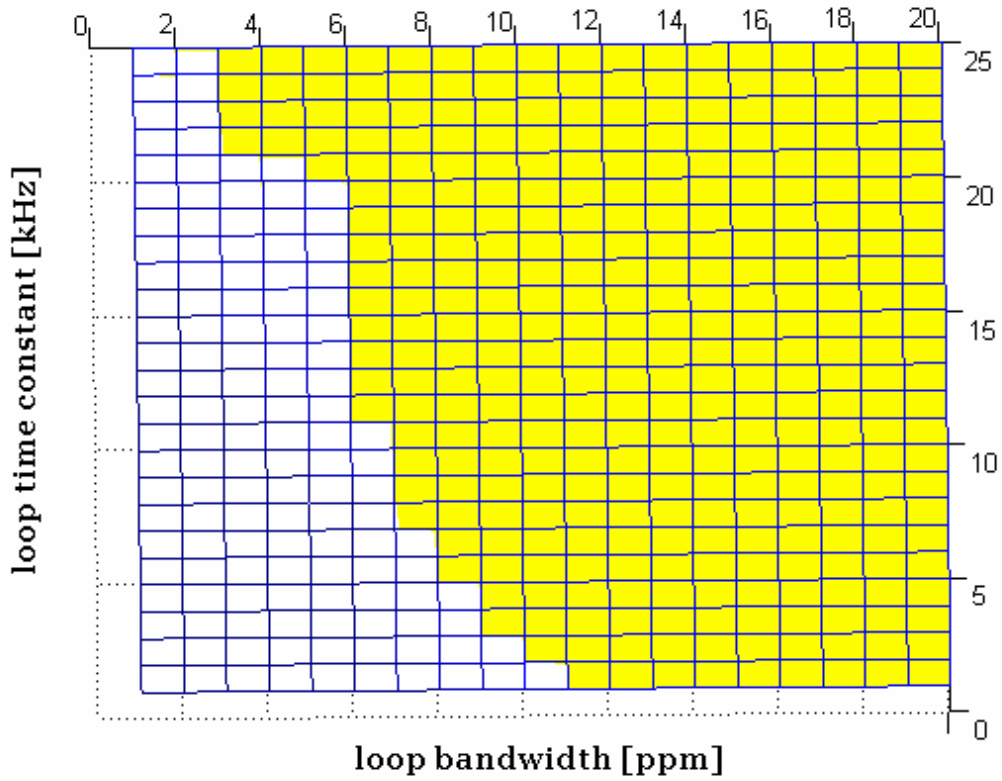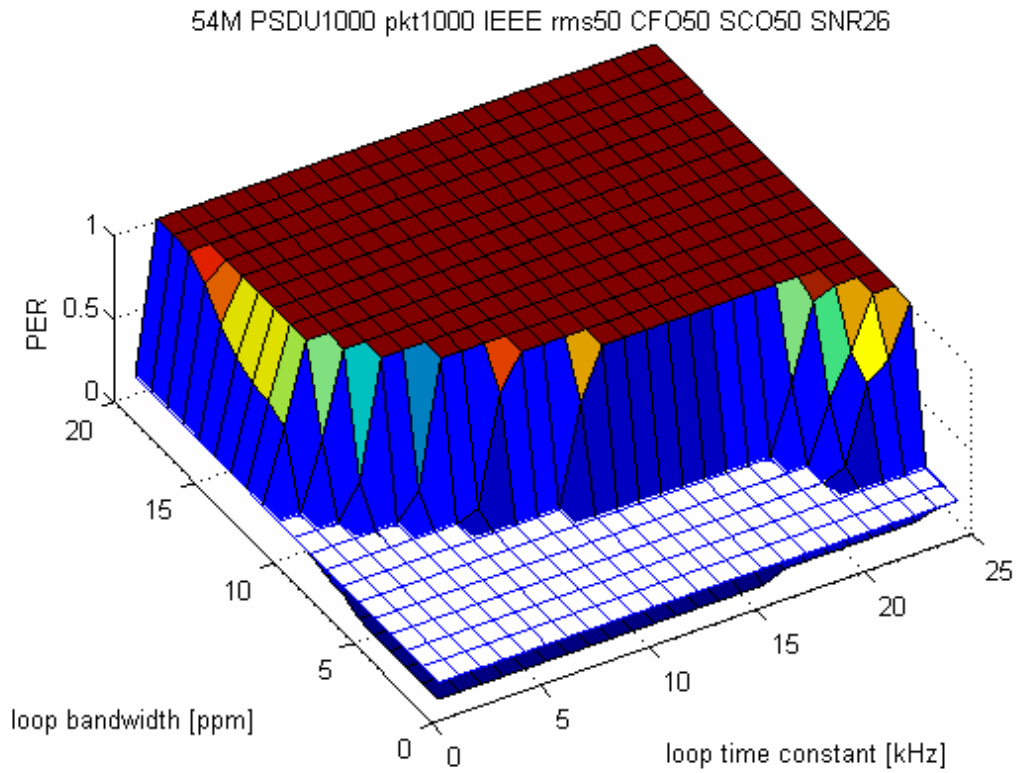**Figure 4.8** Performance without phase noise detector and the profile when PER = 1.

Figure 4.9 Performance with phase noise detector and the profile when PER = 1.

Chapter 5

THE PROPOSED ARCHITECTURE

5.1 Architecture of Adaptive Equalization

The whole architecture of the proposed adaptive equalization can be divided into three parts, the CFR error tracking, the property measurement and the others. The architecture of the algorithm is depicted in Figure 5.1. At first, distorted long preamble is divided the known training symbols in advance. We obtain the initial CFR and put it into the 5-tap smooth filter. The smoothed CFR will be used for data compensation. The CFR error tracking loop contains five components. The upper adder and multiplier are used to calculate normalized de-mapping error vector. Then the results representing the mean of normalized constellation error vectors will be stored in the accumulator. After multiplying the smoothed CFR, the residual estimation error is induced. The most important part of this architecture is the property measurement which consists of two pairs of MSE calculator and a comparator. The MSE calculator is composed of one adder, square device, four shift registers and the summation block. As implied by the name, it computer the MSE of the equalized pilots and the desired pilots. In the end, the comparator will decide if we should update the CFR, since this output of the property measurement controls the multiplexer for equalization. The hardware cost listed in Table 5.1 includes four multipliers, four adders and about 162 kilo-bytes memory space.
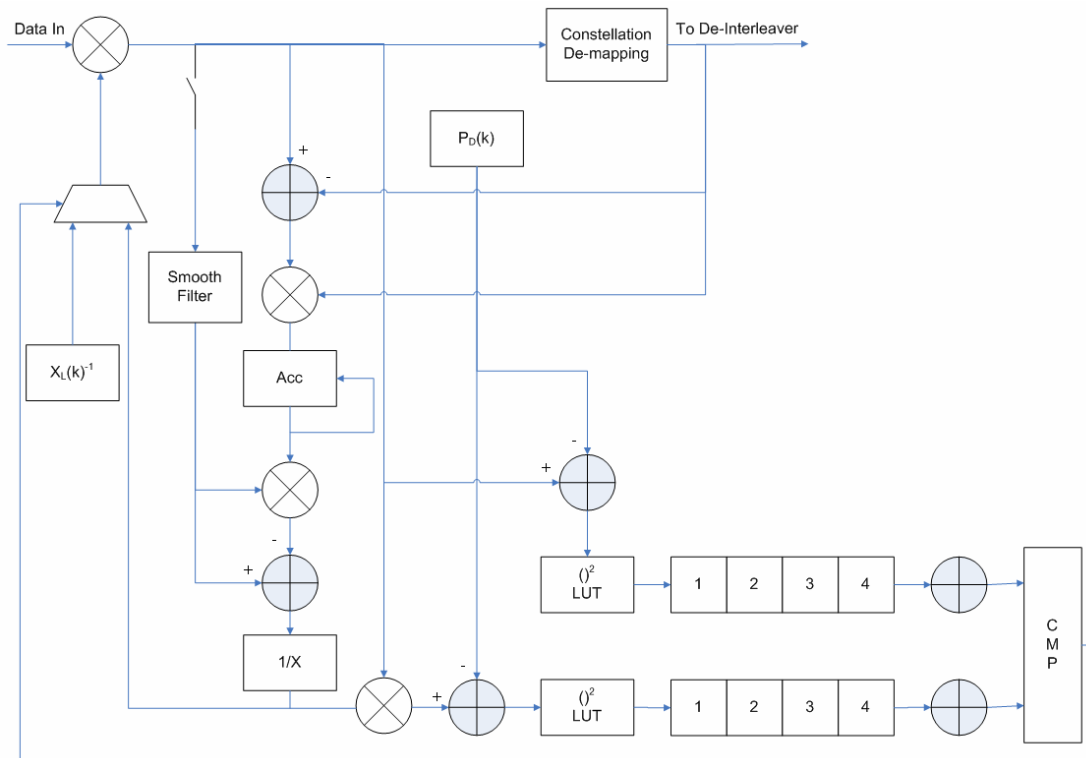
Figure 5.1 The hardware architecture of adaptive equalization.

Table 5.1 Hardware complexity of the proposed adaptive equalization.

	Multiplier	Adder	Register (B)
Quantity	4	6	1.6 k

5.2 Architecture of Phase Noise Detection

Figure 5.2 shows the architecture of the phase noise detection. In the beginning, the residual frequency offset, $C_{0,l}$, and the corresponding OFDM symbol number, l, are delivered form PR. We use the remaining frequency offset to calculate the tendency of the wave came of phase noise as described in section 3.3. The search window is implemented with ten 1-bit shifter registers. The half of the registers is added then compared with the error threshold for search peak. Here the threshold is set to 3 over 5, which mean we can declare the peak is found if there are at least three in five taps. As soon as peak is found, the corresponding symbol number is passed to the table for estimating loop time constant, $\Delta\omega$. Then we use the result for estimating another parameter. The difference of the remaining frequency offset, their corresponding symbol numbers and the estimated loop time constant are the input of the table containing formula for computing loop bandwidth. The comparator of upper one is used to control the switch of tracking mechanism. Another comparator is used to avoid the loop bandwidth out of bound and will make B dispersing. The hardware cost of the proposed phase noise detector listed in Table 5.2 includes four adders and 109 bytes memory space in rough. The compensation architecture here is ignored because it only needs to fix the NCO table for adding sine calculation.
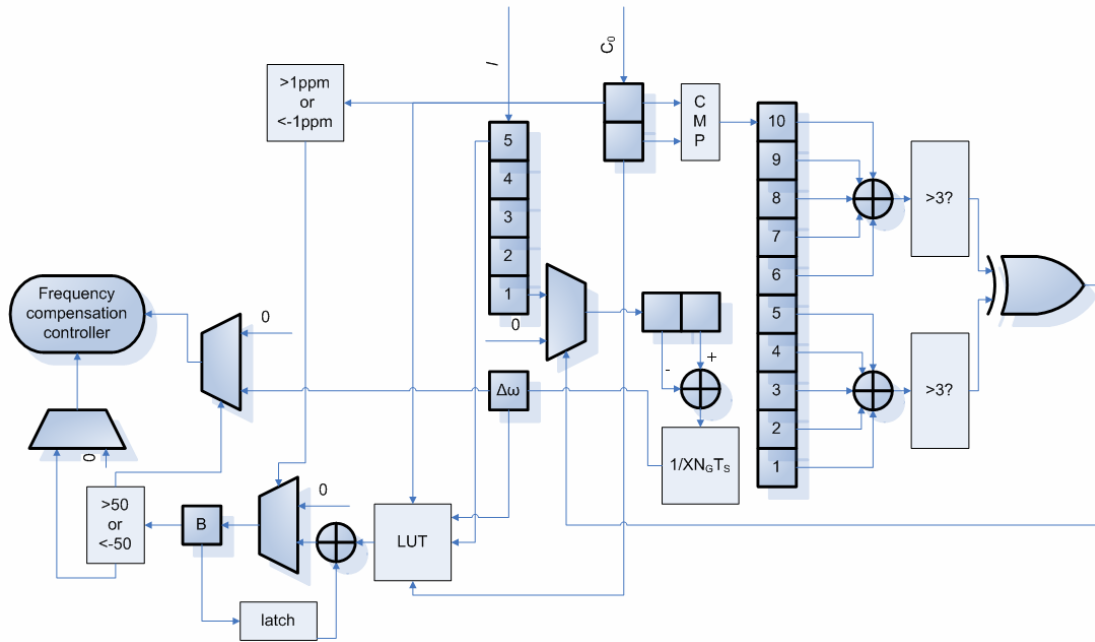
Figure 5.2 The hardware architecture of phase noise detection.

Table 5.2 Hardware complexity of the proposed phase noise detection.

	Multiplier	Adder	Register (B)
Quantity	0	4	109

Chapter 6

CONCLUSION AND FUTURE WORK

6.1 Conclusion

This thesis proposes a novel scheme for channel equalization in OFDM receivers. The proposed algorithm can use de-mapping results and pilots to adjusting estimate channel frequency response in singular multipath environments. From simulation results, the average estimation error of the proposed algorithm is small enough for little system performance loss under different multipath channel. And the convergence speed is much faster at the same time. Besides, the proposed method is suitable for implementation issue compared with the reference designs.

By the way, a phase noise with CFO model is also constructed in this thesis. It is found that the joint effects of phase noise and CFO degrade the system performance dramatically. Thus we propose a novel estimation algorithm and a robust compensation scheme which is shown to work well under loop bandwidth 11 ppm, loop time constant 25 kHz, and maximum CFO tolerance 50 ppm at 2.4 GHz carrier frequency. All of the estimations are done in the known pilots.

Therefore, the proposed algorithm can enhance the performance of OFDM systems and is possible to achieve both small and low-cost systems.

6.2 Future Work

In the future, high QAM constellation which will be more sensitive to non-ideal effects such as CFO and phase noise may be used for higher data rate. Multi-input

multi-output OFDM (MIMO-OFDM) systems are also gaining prominence in high data rate applications. However, the above problem in this thesis will limit the system performance. That means a more robust scheme has to be applied to overcome these impairments. Although the CFO estimation mechanism is good enough, it still needs some adjustment when IQ mismatch occurs [8]. Besides, computation in low-SNR points for CFO estimation can be eliminated for high performance and low complexity, i.e. coarse tune using two autocorrelations with 4 point per short symbol and fine tune using one autocorrelation with 32 points per long symbol [10].So some extensions to the research presented in this thesis will be included in our future work.

A. In the future, the work is to improve the detection range of the proposed method. Additionally, we will need some mechanism for special case in the proposed method.

B. This thesis proposed the phase noise estimation in single-input single-output OFDM (SISO-OFDM) system. In the future, we will try to derive a model for the effect of phase noise and CFO in MIMO-OFDM system and develop a compensation technique for the impairment.

References

[1] IEEE 802.11a, IEEE Standard for Wireless LAN Medium Access Control and Physical Layer Specifications, Dec. 1999.

[2] IEEE 802.11b, IEEE Standard for Wireless LAN Medium Access Control and Physical Layer Specifications, Sept. 1999.

[3] IEEE 802.11g, IEEE Standard for Wireless LAN Medium Access Control and Physical Layer Specifications, June 2003.

[4] Hung-Kuo Wei, *A Frequency estimation and compensation method for high speed OFDM-based WLAN system*, National Chiao Tung University, Taiwan, June 2003, Master's thesis.

[5] Takeshi Onizawa, Masato Mizoguchi, Tetsu Sakata, Masahiro Morikura, "A simple adaptive channel estimation scheme for OFDM systems," in *Proc. IEEE Vehicular Technology Conference (VTC 1999-Fall)*, vol. 1, pp. 19-22 Sept. 1999.

[6] Sun-Wook Kim, Kyun-Hyon Tchah, "Performance analysis of adaptive equalizer design for OFDM wireless LAN," *IEEE Transactions on Consumer Electronics*, vol. 50, pp. 512-516, May 2004.

[7] Yi-Hsin Yu, *A Channel Equalizer for OFDM-based Wireless Access Systems*, National Chiao Tung University, Taiwan, June 2004, Master's thesis.

[8] Ming-Fu Sun, *Joint Estimation and Compensation of I/Q Mismatch and Carrier Frequency Offset in OFDM Systems*, National Chiao Tung University, Taiwan, June 2005, Master's thesis.

[9] Chien-Jen Hung, *A Differential Decoding Based Baseband Processor for DSSS Wireless LAN Applications*, National Chiao Tung University, Taiwan, June 2003,

Mater's thesis.

[10] Lin-Hung Chen, *A Low Complexity Frequency Synchronizer for OFDM-based Wireless Access Applications*, National Chiao Tung University, Taiwan, June 2005, Mater's thesis.

[11] John Terry and Juha Heiskala, *OFDM Wireless LANs: A Theoretical and Practical Guide*. Sams, Indianapolis, Indiana, 2002, ISBN 0-672-32157-2.

[12] Zhiguo Zhang, Shing-Chow Chan, Hui Cheng, "Robust Adaptive Channel Estimation of OFDM Systems in Time-Varying Narrowband Interference," in *Proc. IEEE International Symposium on Circuits and Systems (ISCAS 2005)*, pp. 1722-1725, May 2005.

[13] Xuan Huan Nguyen, Jinho Choi, "Reduced-rank adaptive time-domain channel estimation for OFDM systems," in *Proc. IEEE International Conference on Communications Systems (ICCS 2004)*, pp.135-139, Sept. 2004.

[14] Taewoo Han, Xiaohua Li, "Blind adaptive equalization of OFDM transmission with insufficient cyclic prefix," in *Proc. IEEE International Conference on Modern Problems of Radio Engineering, Telecommunications and Computer Science (TCSET 2004)*, pp. 213-216, Feb. 2004.

[15] Hewavithana, T.C., Brookes, D.A., "Blind adaptive channel equalization for OFDM using the cyclic prefix data," in *Proc. IEEE Global Telecommunications Conference (GLOBECOM'04)*, vol.4, pp. 2376-2380, Nov./Dec. 2004.

[16] Fan Yang, Wee Ser, "Adaptive semi-blind channel estimation for OFDM systems", in *Proc. IEEE Vehicular Technology Conference (VTC 2004-Spring)*, vol.3, pp. 1773-1776, May 2004.

[17] Doukopoulos, X.G., Moustakides, G.V., "Adaptive algorithms for blind channel estimation in OFDM systems", in *Proc. IEEE International Conference on Communications (ICC 2004)*, vol.4, pp. 2377-2381, June 2004.

[18] K. Fazel, S. Kaiser, *Multi-Carrier and Spread Spectrum Systems*. Wiley, 2003, ISBN 0-470-84899-5.

[19] Moose, P.H., "A technique for orthogonal frequency division multiplexing frequency offset correction," *IEEE Transactions on Communications*, vol. 42, pp. 2908-2914, Oct. 1994.

[20] Shynk, J.J, "Frequency-domain and Multirate adaptive filtering", *IEEE Signal Processing Magazine*, vol. 9, pp. 14-37, Jan. 1992.

[21] Eur. Telecommun. Stand., *Radio Broadcasting Systems: Digital Audio Broadcasting to Mobile, Portable and Fixed Receivers*, Feb.1995.

[22] Eur. Telecommun. Stand., *Digital Vedio Broadcasting: Framing Structure, Channel Coding, and Modulation for Digital Terrestrial Television*, Aug. 1997.

[23] Garcia Armada, A, "Understanding the effects of phase noise in orthogonal frequency division multiplexing (OFDM)," *IEEE Transactions on Broadcasting*, vol. 47, pp.135–159, June 2001.